

GW Detection in Space: An Overview

Wei-Tou Ni 倪维斗

National Tsing Hua University

Refs: [WTN, GW detection in space](#) IJMPD 25 (2016) 1530002

Chen, Nester, and WTN, Chin J Phys 55 (2017) 142-169

K Kuroda, WTN, WP Pan, IJMPD 24 (2015) 1530031;

Outline

- INTRODUCTION – Science goals
- A brief history and technology development
- Space Interferometric GW mission proposals
- Orbit configuration and TDI (time delay interferometry)
- Other space detection proposals
- OUTLOOK

Gravitational Waves – Ripples in Spacetime

- Monochromatic

A single frequency plane GW

- Wave form in time t ,

Spectral form in frequency f

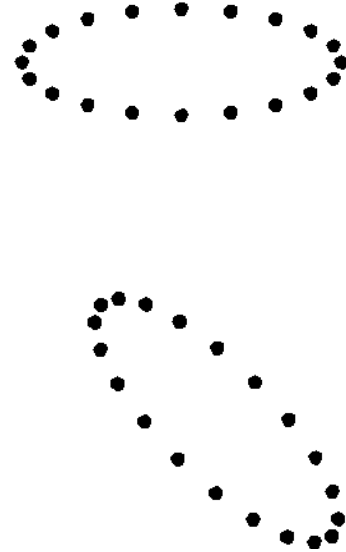
- Noise power amplitude

$$\langle n^2(t) \rangle = \int_0^\infty (df) S_n(f), \quad h_n(f) \equiv [f S_n(f)]^{1/2}$$

- Characteristic amplitude

$$h_{\mu\nu}(U) = \int_0^\infty 2 |{}^{(f)}h_{\mu\nu}(f)| \cos(2\pi f U/c) (df) \\ = \int_0^\infty 2f |{}^{(f)}h_{\mu\nu}(f)| \cos(2\pi f U/c) d(\ln f).$$

$$h_c(f) \equiv 2f [(|{}^{(f)}h_{\times}(f)|^2 + |{}^{(f)}h_{\times}(f)|^2)]^{1/2}; \quad h_{cA}(f) \equiv 2f |{}^{(f)}h_{\times}(f)|$$



$$A_{\mu,\beta}{}^\beta = 4\pi J_\mu,$$

with gauge condition

$$A_{\alpha,\alpha} = 0.$$

$$h_{\mu\nu} = -[(4G_N)/(c^4)] \int \{ [T_{\mu\nu} - (1/2) g_{\mu\nu} T] / r \}_{\text{retarded}} (d^3x') + O(h^2)$$

The retarded solution of equation (12) is

$$A_\mu = \int (J_\mu / r)_{\text{retarded}} (d^3x').$$

$$[\epsilon^{(1)}]_{ij} = \begin{pmatrix} 0 & 0 & 0 \\ 0 & 0 & 0 \\ 0 & 0 & 1 \end{pmatrix} \quad [\epsilon^{(2)}]_{ij} = \begin{pmatrix} 0 & 0 & 1 \\ 0 & 0 & 0 \\ 1 & 0 & 0 \end{pmatrix} \\ [\epsilon^{(3)}]_{ij} = \begin{pmatrix} 0 & 0 & 0 \\ 0 & 0 & 1 \\ 0 & 1 & 0 \end{pmatrix} \quad [\epsilon^{(4)}]_{ij} = \begin{pmatrix} 1 & 0 & 0 \\ 0 & -1 & 0 \\ 0 & 0 & 0 \end{pmatrix} \\ [\epsilon^{(5)}]_{ij} = \begin{pmatrix} 0 & 1 & 0 \\ 1 & 0 & 0 \\ 0 & 0 & 0 \end{pmatrix} \quad [\epsilon^{(6)}]_{ij} = \begin{pmatrix} 1 & 0 & 0 \\ 0 & 1 & 0 \\ 0 & 0 & 0 \end{pmatrix}.$$

GW propagation direction: z

$$G_{\mu\nu} = \kappa T_{\mu\nu}, \quad R_{\mu\nu} = 8\pi G_N [T_{\mu\nu} - (1/2)(g_{\mu\nu}T)]$$

$$h_{\mu\nu,\beta}{}^\beta = -16\pi G_N [T_{\mu\nu} - (1/2)(\eta_{\mu\nu}T)] + O(h^2)$$

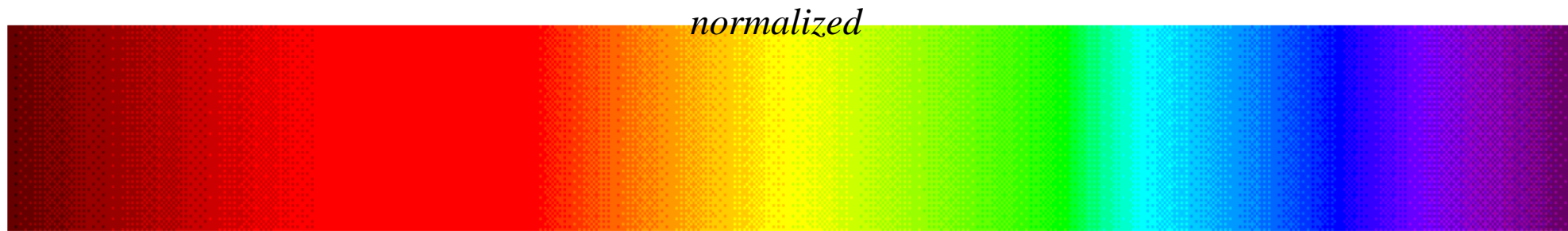
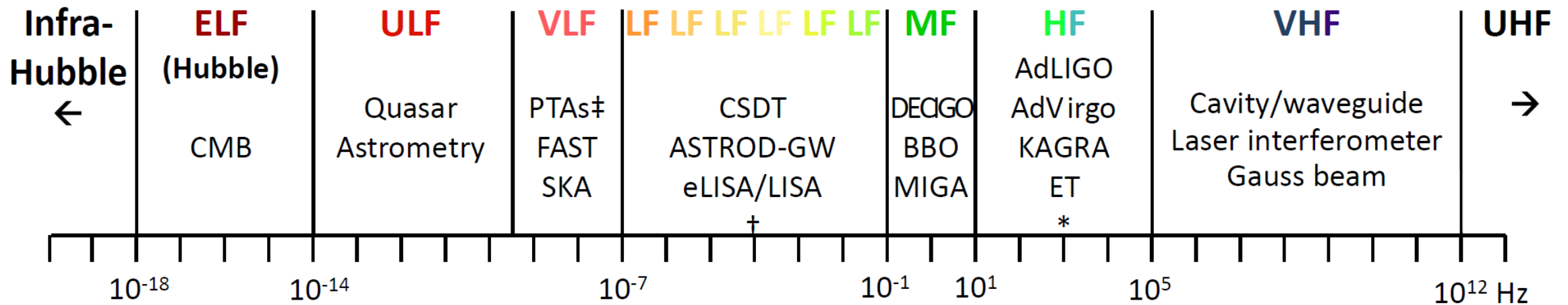
In harmonic gauge

$$\text{plane GW } h_{\mu\nu}(n_x x + n_y y + n_z z - ct) = h_{\mu\nu}(U)$$

$$h_{\mu\nu}(u, t) \equiv h_{\mu\nu}(U) = \int_{-\infty}^\infty {}^{(f)}h_{\mu\nu}(f) \exp(2\pi i f U/c) (df) = \int_0^\infty 2f |{}^{(f)}h_{\mu\nu}(f)| \cos(2\pi f U/c) d(\ln f)$$

$$h_{\mu\nu}(x, y, z, t) = (c/2\pi)^3 \int {}^{(k)}h_{\mu\nu}(k_x, k_y, k_z) \exp(ik_x x + ik_y y + ik_z z - 2\pi i f t) (dk_x dk_y dk_z)$$

引力波谱分类 The Gravitation-Wave (GW) Spectrum Classification



* AIGO, AURIGA, EXPLORER, GEO, NAUTILUS, MiniGRAIL, Schenberg.

† OMEGA, gLISA/GEOGRAWI, GADFLI, TIANQIN, ASTROD-EM, LAGRANGE, ALIA, ALIA-descope.

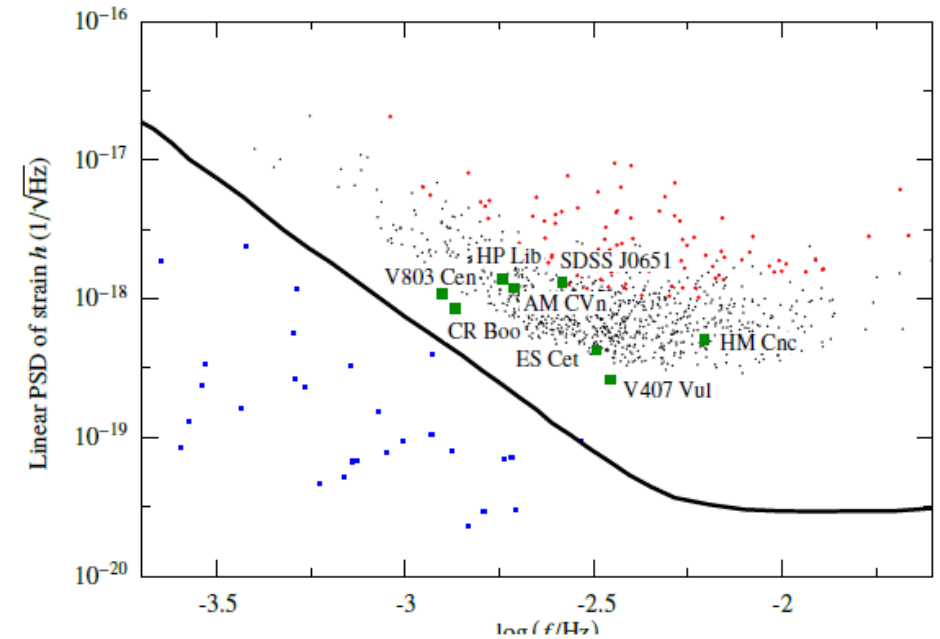
‡ EPTA, NANOGrav, PPTA, IPTA.

Scope: Goals –GW Astronomy & Fundamental Physics

Frequency band	GW sources / Possible GW sources	Detection method
Ultrahigh frequency band: above 1 THz	Discrete sources, Cosmological sources, Braneworld Kaluza-Klein (KK) mode radiation, Plasma instabilities	Terahertz resonators, optical resonators, and magnetic conversion detectors
Very high frequency band: 100 kHz – 1 THz	Discrete sources, Cosmological sources, Braneworld Kaluza-Klein (KK) mode radiation, Plasma instabilities	Microwave resonator/wave guide detectors, laser interferometers and Gaussian beam detectors
High frequency band (audio band)*: 10 Hz – 100 kHz	Compact binaries [NS (Neutron Star)-NS, NS-BH (Black Hole), BH-BH], Supernovae	Low-temperature resonators and Earth-based laser-interferometric detectors
Middle frequency band: 0.1 Hz – 10 Hz	Intermediate mass black hole binaries, massive star (population III star) collapses	Space laser-interferometric detectors of arm length 1,000 km – 60,000 km
Low frequency band (milli-Hz band)†: 100 nHz – 0.1 Hz	Massive black hole binaries, Extreme mass ratio inspirals (EMRIs), Compact binaries	Space laser-interferometric detectors of arm length longer than 60,000 km
Very low frequency band (nano-Hz band): 300 pHz – 100 nHz	Supermassive black hole binary (SMBHB) coalescences, Stochastic GW background from SMBHB coalescences	Pulsar timing arrays (PTAs)
Ultralow frequency band: 10 fHz – 300 pHz	Inflationary/primordial GW background, Stochastic GW background	Astrometry of quasar proper motions
Extremely low (Hubble) frequency band: 1 aHz–10 fHz	Inflationary/primordial GW background	Cosmic microwave background experiments
Beyond Hubble-frequency band: below 1 aHz	Inflationary/primordial GW background	Through the verifications of primordial cosmological models

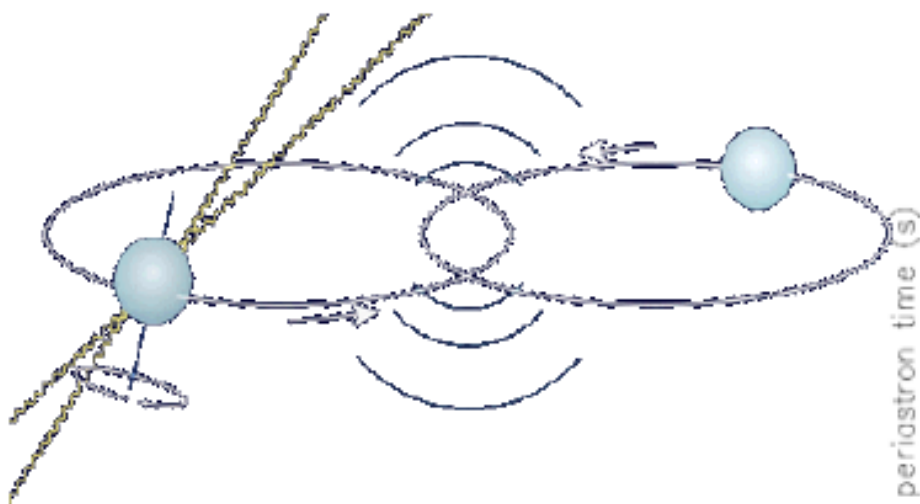
Observation-Tech Gap 100 years ago

- 1916, 1918 Einstein predicted GW and derived the quadrupole radiation formula
- White dwarf discovered in 1910 with its density soon estimated; GWs from white dwarf binaries in our Galaxy form a stochastic GW background
(confusion limit for space GW detection: strain, 10^{-20} in 0.1-1mHz band).
[Periods: 5.4 minutes (HM Cancri) to hours](3 mHz)
- One hundred year ago, the sensitivity of astrometric observation through the atmosphere around this band is about 1 arcsec. This means the strain sensitivity to GW detection is about 10^{-5} ; 15 orders away from the required sensitivity.
- Observation-Tech Gap 100 years ago: 15 orders

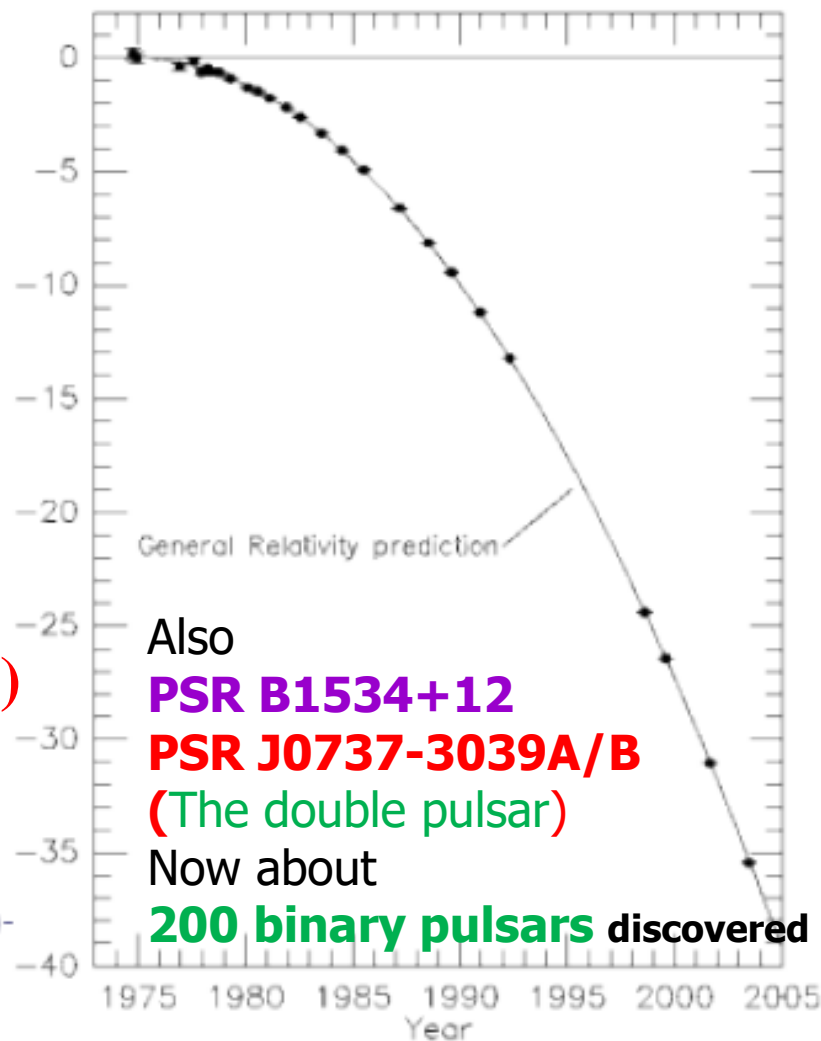


Hulse-Taylor Binary PSR1913+16

国际暨中德双边激光天文动力学研讨会



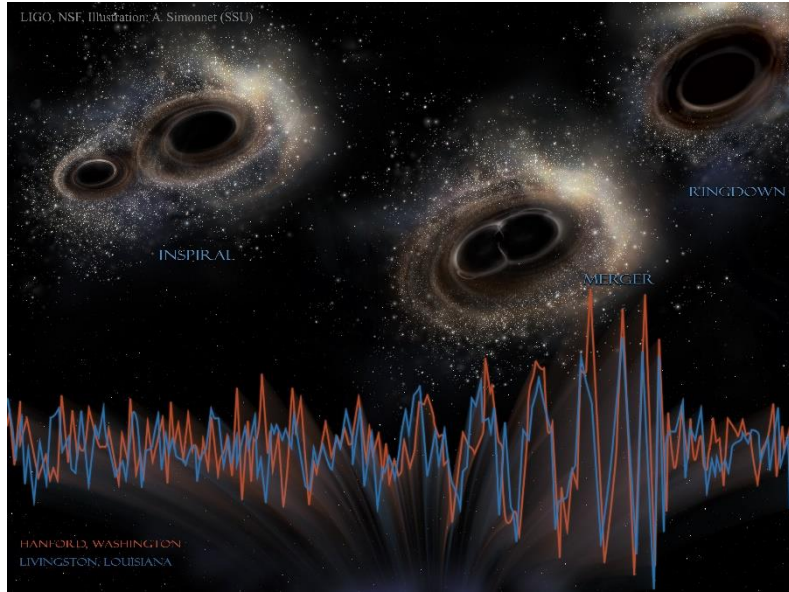
- Observed loss of energy matches prediction of GW emission to $(0.13 \pm 0.21)\%$ **$0.997 \pm 0.002 (2010)$**
- Indirect evidence of gravitational waves
- Frequency $70 \mu\text{Hz}$, amplitude $7 \times 10^{-23} \Rightarrow$ outside detector sensitivity



The observation and technology gap 100 years ago in the 10 Hz – 1 kHz band

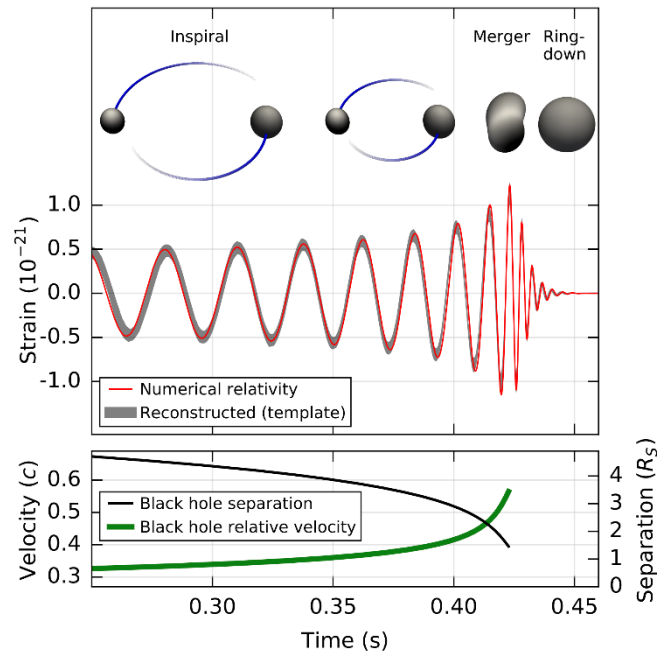
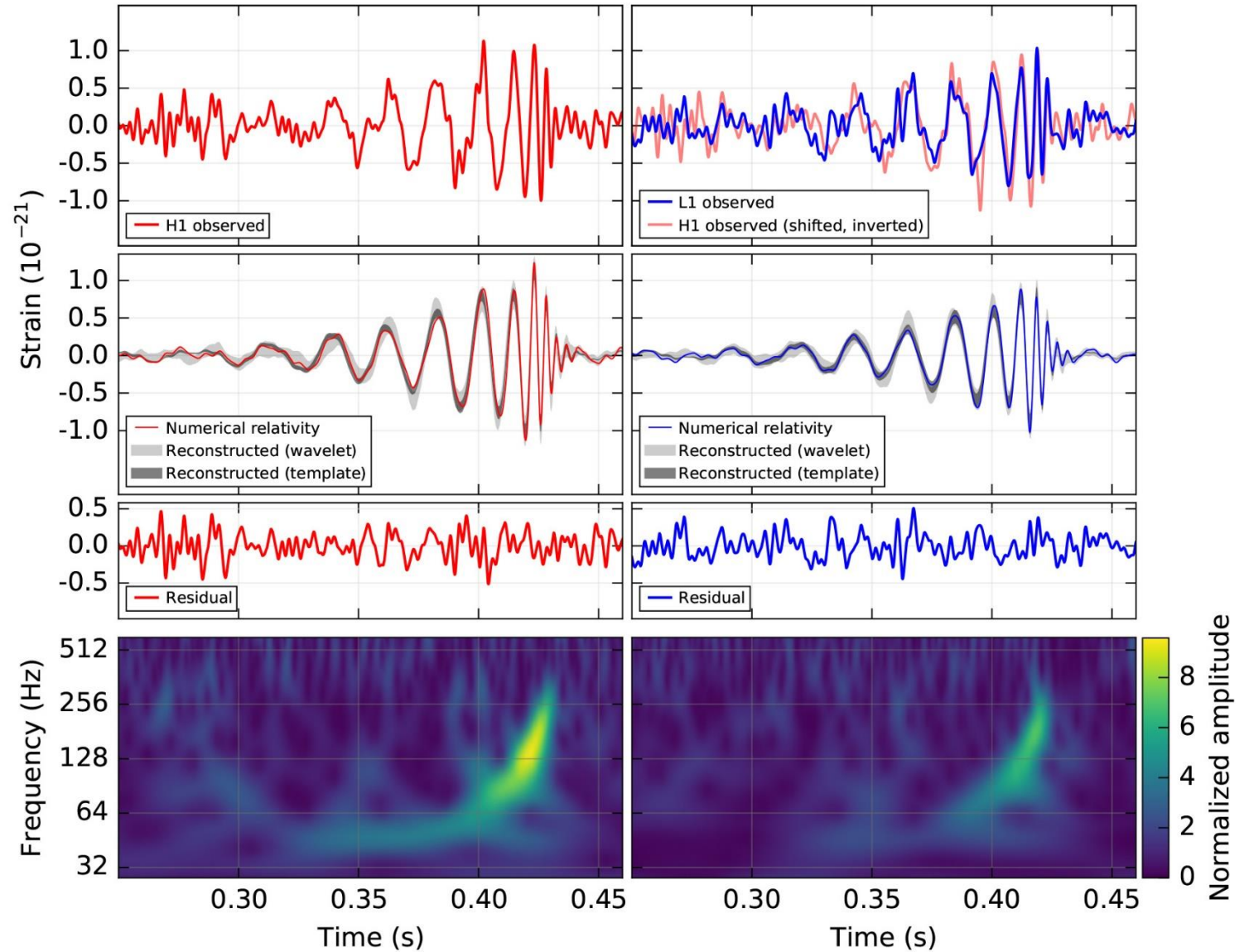
- In the LIGO discovery of 2 GW events and 1 probable GW candidate, the maximum peak strain intensity is 10^{-21} ; the frequency range is 30-450 Hz.
- Strain gauge in this frequency region could reach 10^{-5} with a fast recorder about 100 years ago;
- thus, the technology gap would be 16 orders of magnitudes.
- Michelson interferometer for Michelson-Morley experiment¹⁰ has a strain ($\Delta l/l$) sensitivity of 5×10^{-10} with 0.01 fringe detectability and 11 m path length;
- however, the appropriate test mass suspension system with fast (30-450 Hz in the high-frequency GW band) white-light observing system is lacking.

2016年2月11日宣布首探 Announcement of first detection

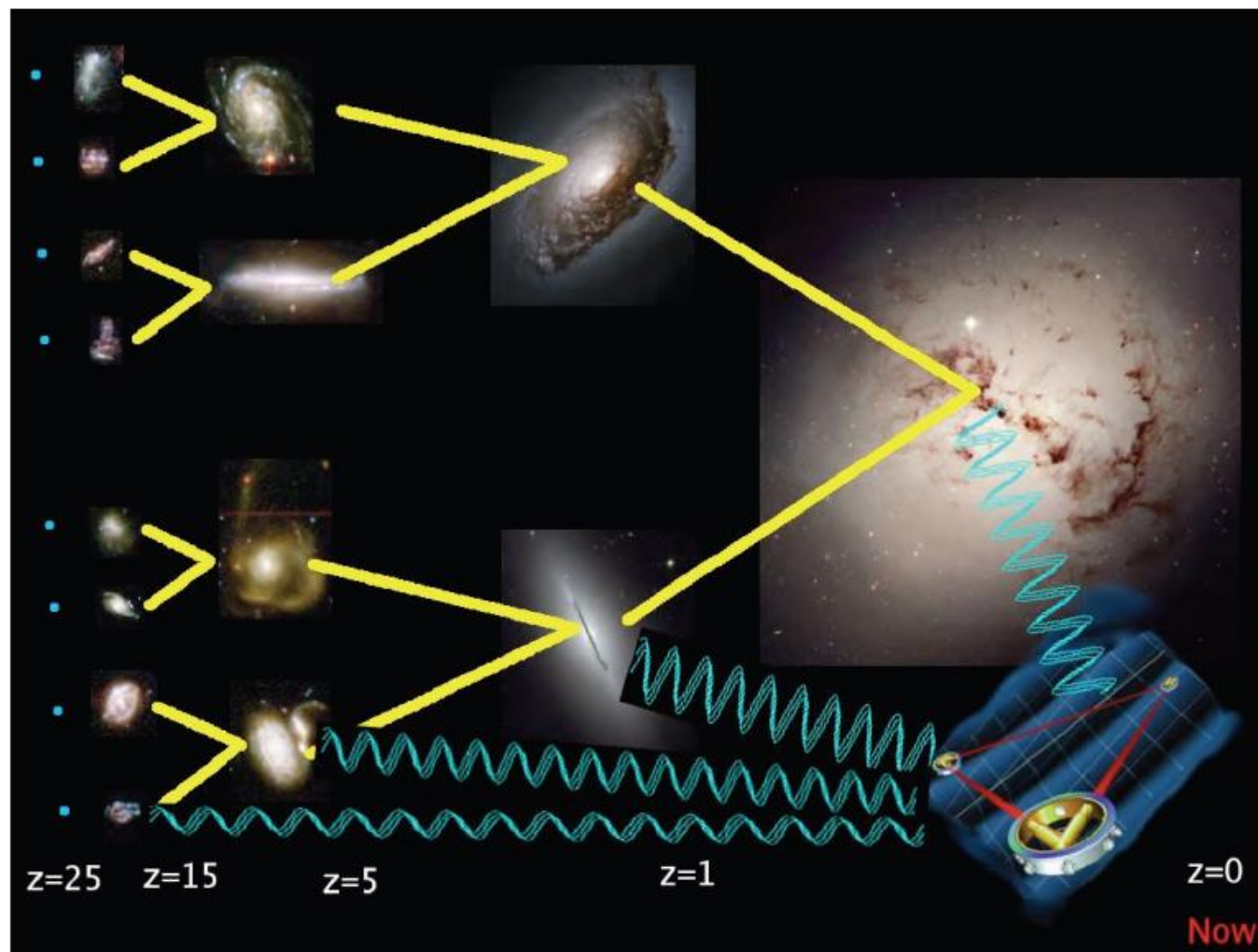


Hanford, Washington (H1)

Livingston, Louisiana (L1)



Massive Black Hole Systems: Massive BH Mergers & Extreme Mass Ratio Mergers (EMRIs)



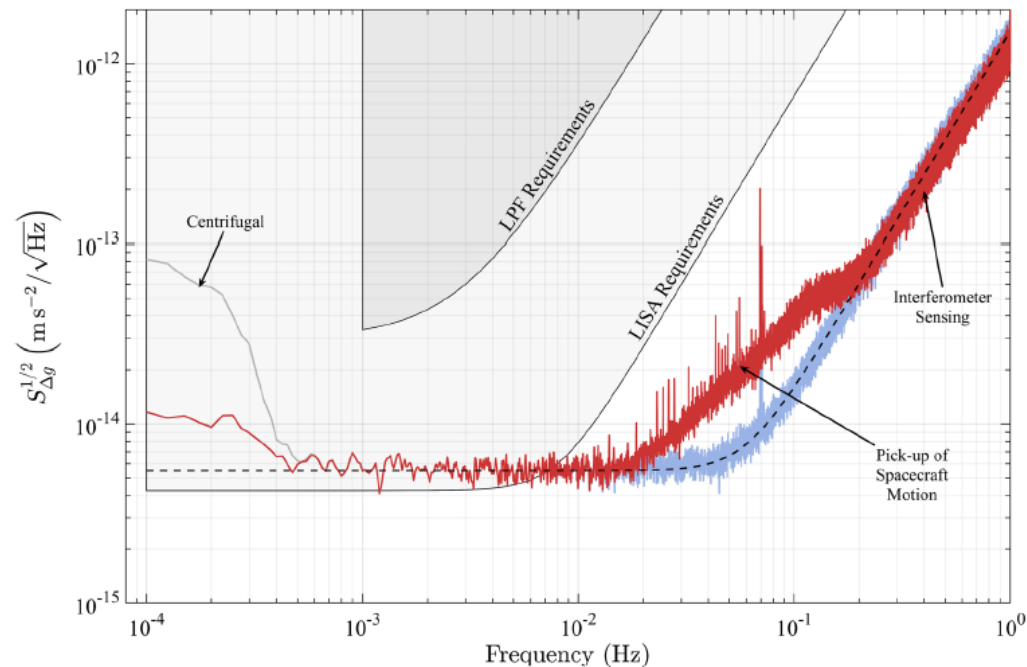
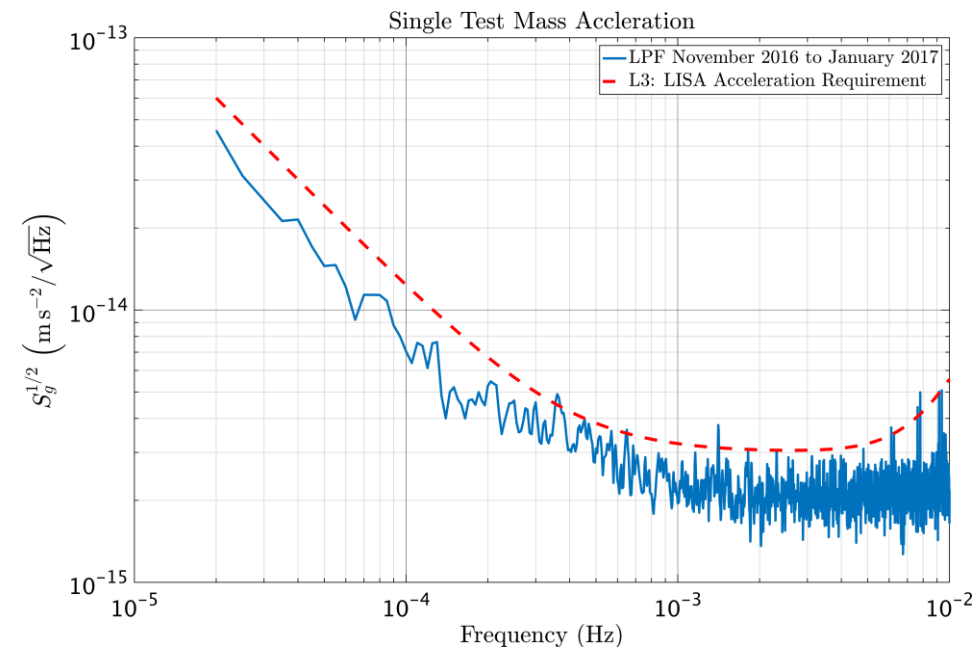
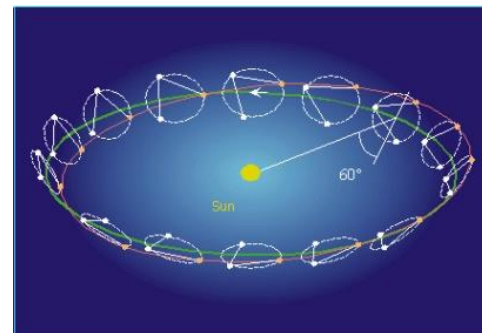
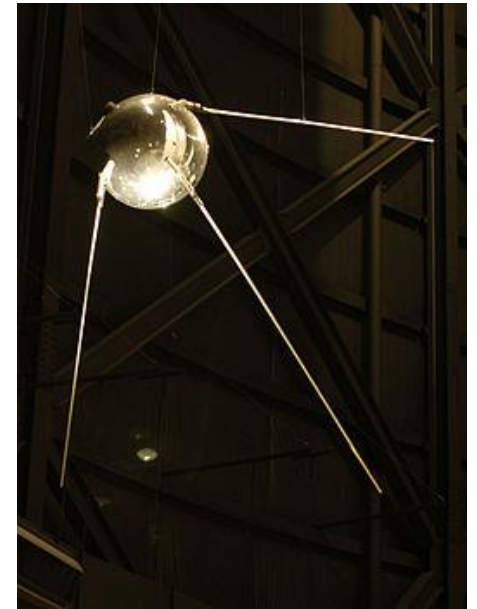
Science Goals

- The science goals are the detection of GWs from
 - (i) Supermassive Black Holes;
 - (ii) Extreme-Mass-Ratio Black Hole Inspirals;
 - (iii) Intermediate-Mass Black Holes;
 - (iv) Galactic Compact Binaries;
 - (v) Relic/Inflationary GW Background.

Gap largely bridged

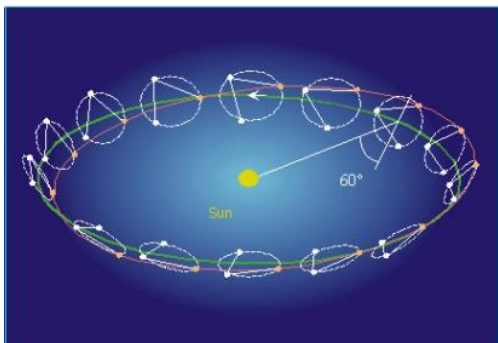
92 days
1440 orbits
83.60 kg mass

- First artificial satellite **Sputnik** launched in **1957**.
- First GW space mission proposed in public in 1981 by Faller & Bender
- LISA proposed as a joint ESA-NASA mission; LISA Pathfinder successfully performed. The drag-free tech is fully demonstrated paving the road for GW space missions.



Weak-light phase locking and manipulation technology

- Weak-light phase locking is crucial for long-distance space interferometry and for CW laser space communication. For **LISA** of arm length of **5 Gm (million km)** the weak-light phase locking requirement is for **70 pW** laser light to phase-lock with an onboard laser oscillator. For **ASTROD-GW** arm length of **260 Gm (1.73 AU)** the weak-light phase locking requirement is for **100 fW** laser light to lock with an onboard laser oscillator. **Weak-light phase locking for 2 pW laser light to 200 μ W local oscillator is demonstrated in our laboratory in Tsing Hua U.⁶ Dick *et al.*⁷ from their phase-locking experiment showed a PLL (Phase Locked Loop) phase-slip rate below one cycle slip per second at powers as low as 40 femtowatts (fW).**



空间引力波探测

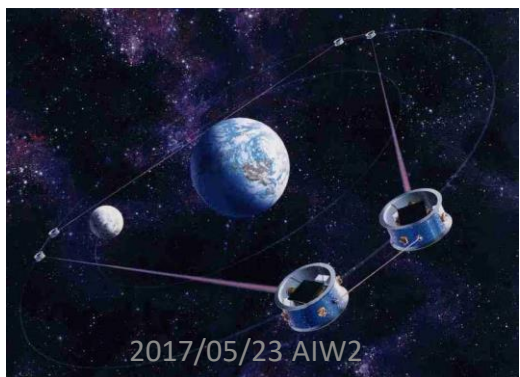
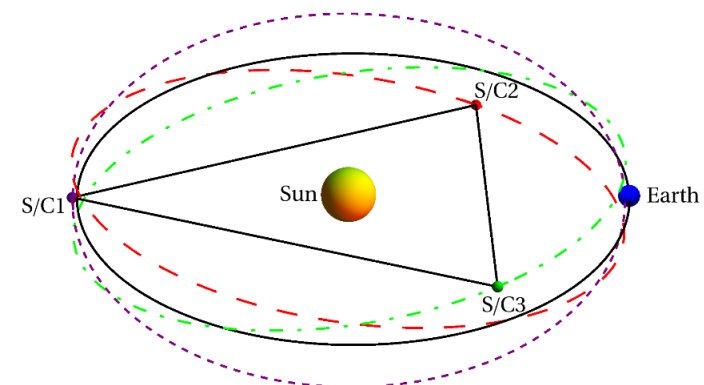
A Compilation of GW Mission Proposals

LISA Pathfinder

Launched on December 3, 2015



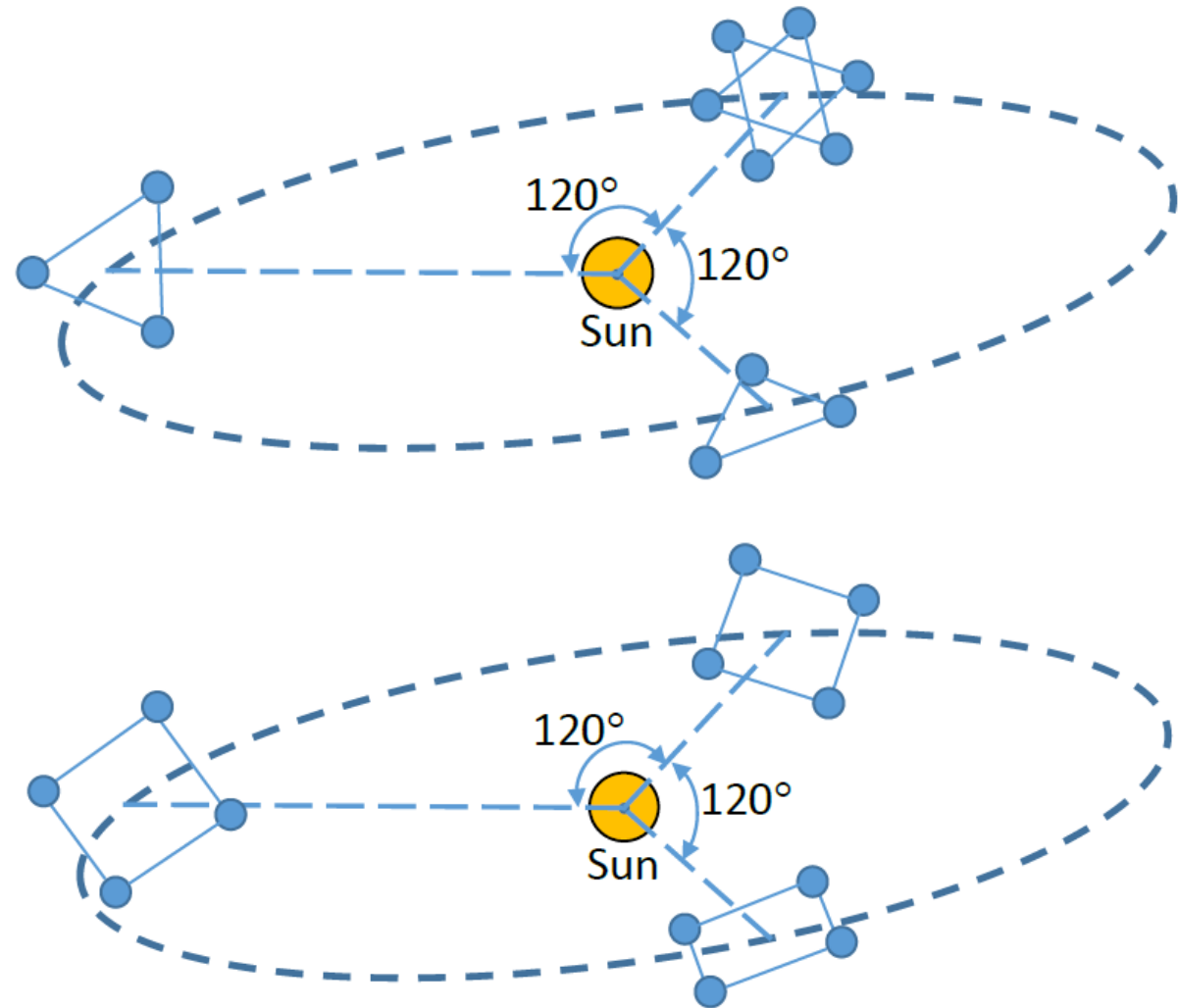
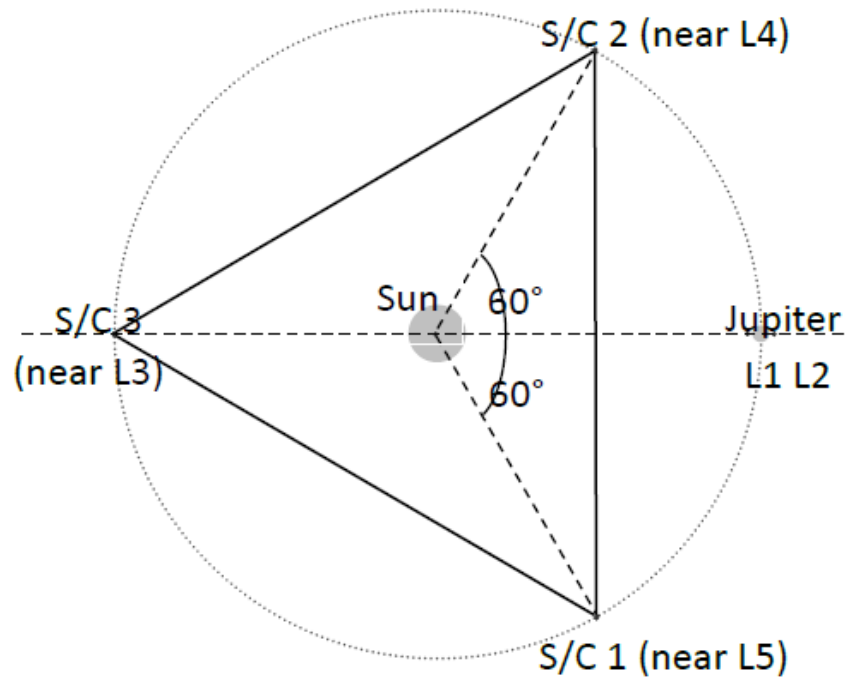
Mission Concept	S/C Configuration	Arm length	Orbit Period	S/C #
<i>Solar-Orbit GW Mission Proposals</i>				
LISA ⁶⁵	Earth-like solar orbits with 20° lag	5 Gm	1 year	3
eLISA ⁶⁴	Earth-like solar orbits with 10° lag	1 Gm	1 year	3
ASTROD-GW ⁶⁸	Near Sun-Earth L3, L4, L5 points	260 Gm	1 year	3
Big Bang Observer ⁷³	Earth-like solar orbits	0.05 Gm	1 year	12
DECIGO ⁷²	Earth-like solar orbits	0.001 Gm	1 year	12
ALIA ⁷⁴	Earth-like solar orbits	0.5 Gm	1 year	3
ALIA-descope ⁷⁵ 太极	Earth-like solar orbits	3 Gm	1 year	3
Super-ASTROD ⁷¹	Near Sun-Jupiter L3, L4, L5 points (3 S/C), Jupiter-like solar orbit(s)(1-2 S/C)	1300 Gm	11 year	4 or 5
<i>Earth-Orbit GW Mission Proposals</i>				
OMEGA ⁸¹	0.6 Gm height orbit	1 Gm	53.2 days	6
gLISA/GEOGRAWI ⁷⁶⁻⁷⁸	Geostationary orbit	0.073 Gm	24 hours	3
GADFLI ⁷⁹	Geostationary orbit	0.073 Gm	24 hours	3
TIANQIN ⁸² 天琴	0.057 Gm height orbit	0.11 Gm	44 hours	3
ASTROD-EM ^{69,70}	Near Earth-Moon L3, L4, L5 points	0.66 Gm	27.3 days	3
LAGRANGE ⁸⁰ GW Detector in Space	Near Earth-Moon L3, L4, L5 points	0.66 Gm	27.3 days ⁸⁴	3



Mission concept	S/C configuration	Arm length	Orbit period	S/C #	Acceleration noise [fm/s ² /Hz ^{1/2}]	Laser metrology noise [pm/Hz ^{1/2}]
<i>Solar-Orbit GW Mission Proposals</i>						
LISA ⁹	Earthlike solar orbits with 20° lag	5 Gm	1 year	3	3	20
eLISA ²¹	Earthlike solar orbits with 10° lag	1 Gm	1 year	3	3	12(10)
ASTROD-GW ^{36–40}	Near Sun–Earth L3, L4, L5 points	260 Gm	1 year	3	3	1000
Big Bang Observer ⁴⁵	Earthlike solar orbits	0.05 Gm	1 year	12	0.03	1.4×10^{-5}
DECIGO ⁴⁴	Earthlike solar orbits	0.001 Gm	1 year	12	0.0004	2×10^{-6}
ALIA ⁴⁷	Earthlike solar orbits	0.5 Gm	1 year	3	0.3	0.6
TAIJI (ALIA-descope) ⁴⁸	Earthlike solar orbits	3 Gm	1 year	3	3	5–8
Super-ASTROD ⁴²	Near Sun–Jupiter L3, L4, L5 points (3 S/C), Jupiterlike solar orbit(s)(1–2 S/C)	1300 Gm	11 year	4 or 5	3	5000
<i>Earth-Orbit GW Mission Proposals</i>						
OMEGA ^{54,55}	0.6 Gm height orbit	1 Gm	53.2 days	6	3	5
gLISA/GEOGRAWI ^{49–51}	Geostationary orbit	0.073 Gm	24 h	3	3, 30	0.3, 10
GADFLI ⁵²	Geostationary orbit	0.073 Gm	24 h	3	0.3, 3, 30	1
TIANQIN ¹⁹	0.057 Gm height orbit	0.11 Gm	44 h	3	1	1
ASTROD-EM ⁴³	Near Earth–Moon L3, L4, L5 points	0.66 Gm	27.3 days	3	1	1
LAGRANGE ⁵³	Earth–Moon L3, L4, L5 points	0.66 Gm	27.3 days	3	3	5

Second Generation GW Mission Concepts

- DECIGO
- BBO
- Super-ASTROD



Estimated delta-V and propellant mass ratio for solar transfer of S/C (Deployment)

° ahead of Earth in solar orbit	Transfer orbit	Transfer time	Solar transfer delta-V after injection from LEO to solar transfer orbit	Solar transfer propellant mass ratio (Isp = 320 s)
180° (near L3)	Venus flyby transfer	1.3–1.5 year	2.2–2.5 km/s	0.50–0.55
60° (near L4)	Inner Hohmann, 2 Revolutions	1.833 year	1.028 km/s	0.280
300° (–60°) (near L5)	Outer Hohmann, 1 Revolutions	1.167 year	2 km/s	0.47
0–60°	Inner Hohmann, ≤ 2 Revolutions	Less than 1.833 year	Less than 1.028 km/s	Less than 0.280
60°–300°	Venus flyby transfer	1.3–1.5 year	2.2–2.5 km/s	0.50–0.55
300°–360°	Outer Hohmann, 1 Revolutions	Less than 1.167 year	Less than 2 km/s	Less than 0.47

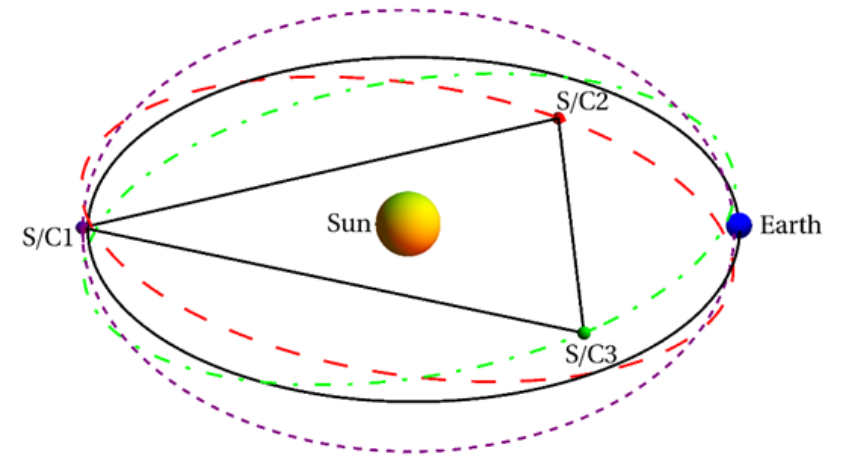
Payload

- Each spacecraft carries a payload of
 - two proof masses,
 - two telescopes,
 - two lasers,
 - a weak light detection and handling system,
 - a laser stabilization system, and
 - a drag-free system.
- For lower part of space GW band or for possibly higher precision, a **precision/optical clock**, or **an absolute laser stabilization system**, and **an absolute laser metrology system** may be used.

Time Delay Interferometry (TDI)

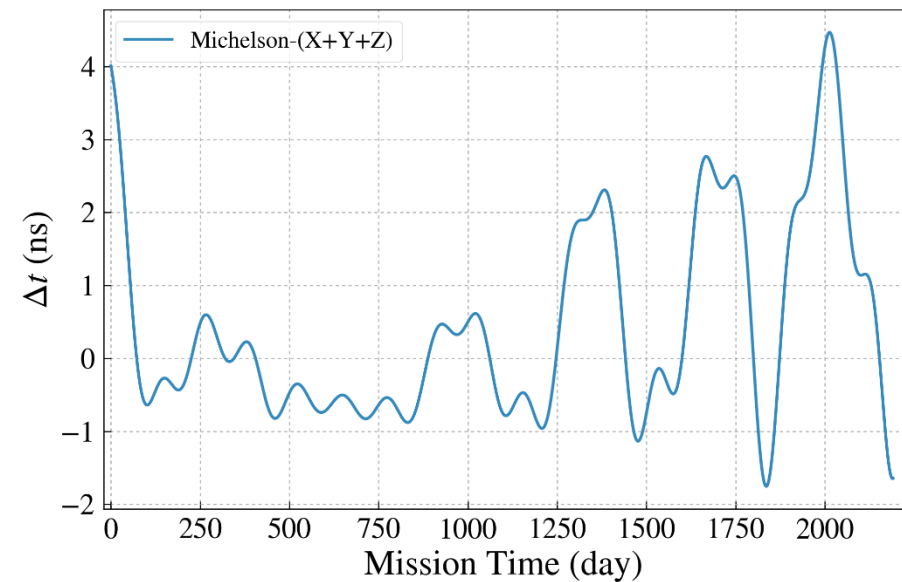
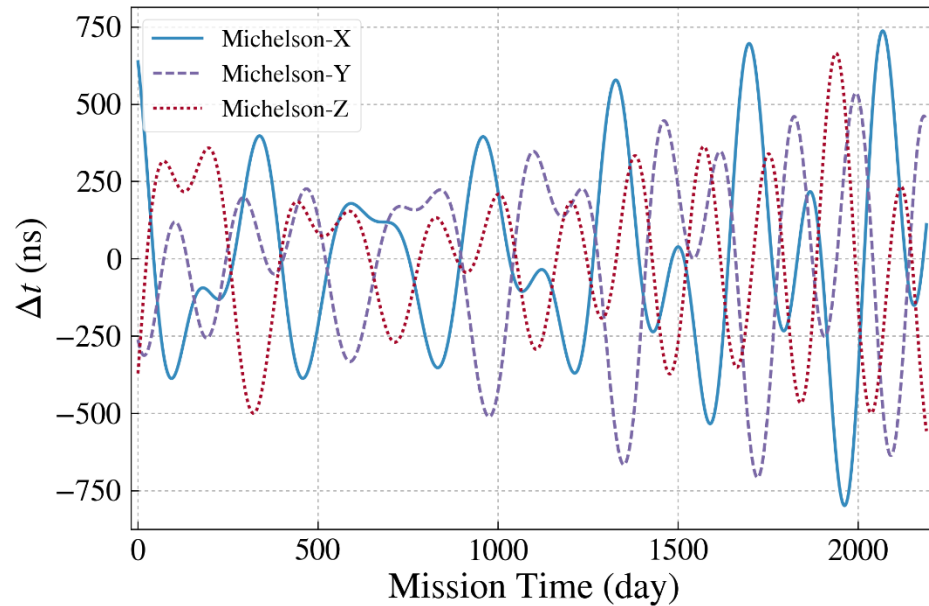
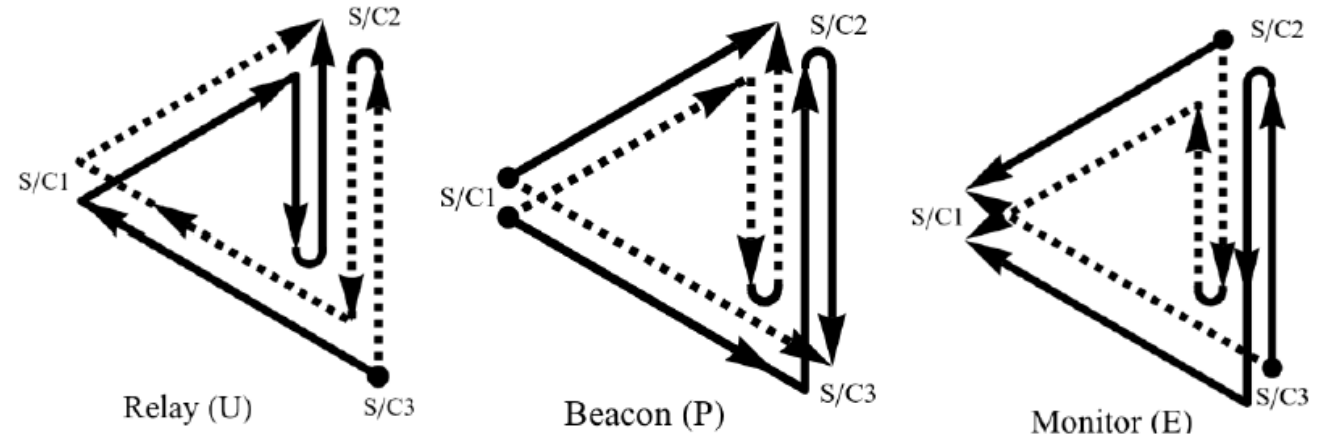
first used in the study of ASTROD mission concept in the 1990s (Ni *et al.* 1997a, 1997b), two TDI configurations were used during the study of ASTROD interferometry and the path length differences were numerically obtained using Newtonian dynamics

- These two TDI configurations are the unequal arm Michelson TDI configuration and the Sagnac TDI configuration for three spacecraft formation flight. The principle is to have two split laser beams to go to Paths 1 and 2 and interfere at their end path. For unequal arm Michelson TDI configuration, one laser beam starts from spacecraft 1 (S/C1) directed to and received by spacecraft 2 (S/C2), and optical phase locking the local laser in S/C2; the phase locked laser beam is then directed to and received by S/C1, and optical phase locking another local laser in S/C1; and so on to return to S/C1:
- Path 1: S/C1 → S/C2 → S/C1 → S/C3 → S/C1. (1)
- The second laser beam starts from S/C1 also:
- Path 2: S/C1 → S/C3 → S/C1 → S/C2 → S/C1, (2)
- to return to S/C1 and to interfere with the first beam.
- If the two paths has exactly the same optical path length,
- the laser frequency noises cancel out; if the optical path length difference is small, the laser frequency noises cancel to a large extent. In the Sagnac TDI configuration, the two paths are:
- Path 1: S/C1 → S/C2 → S/C3 → S/C1, Path 2: S/C1 → S/C3 → S/C2 → S/C1.



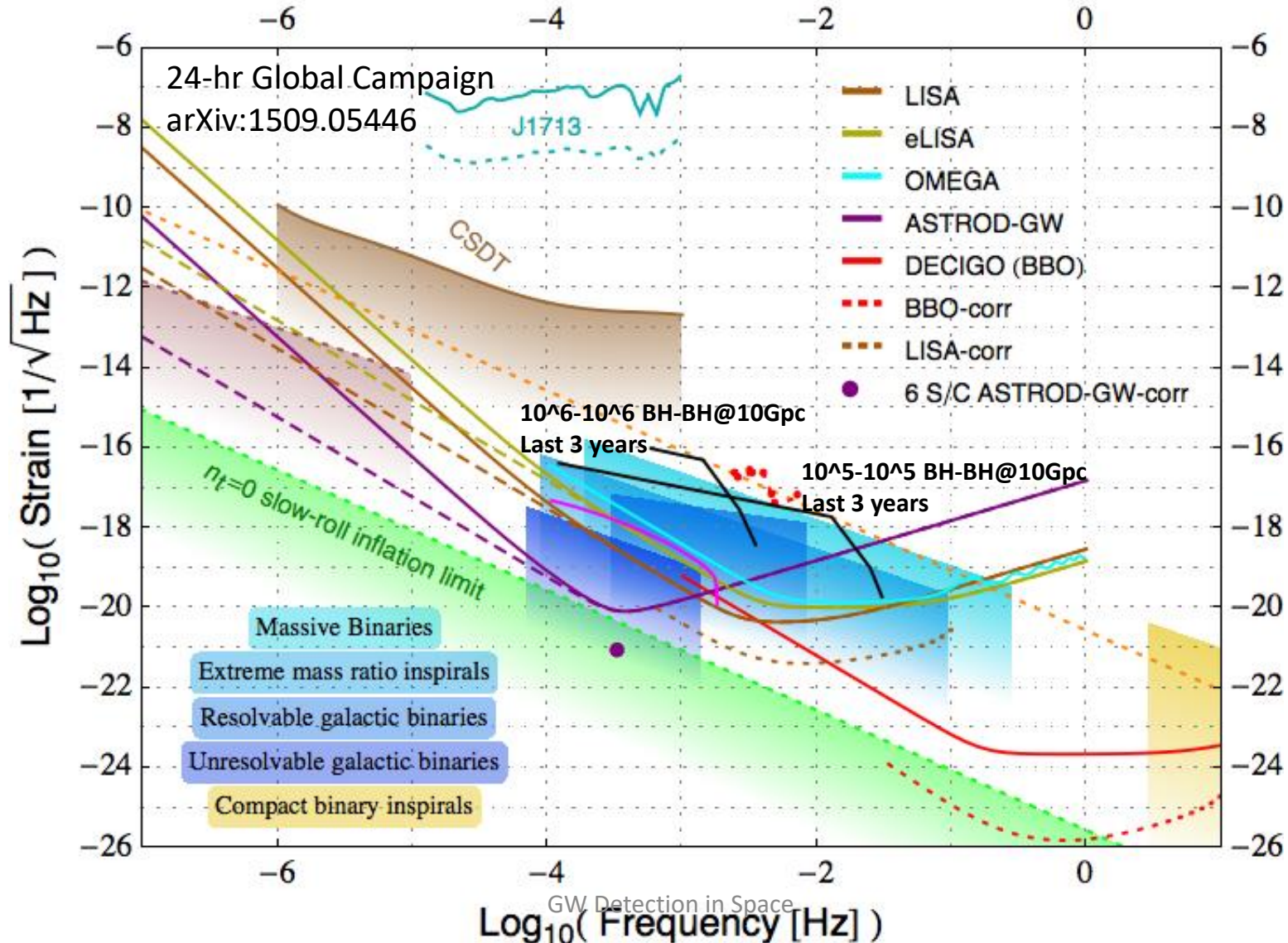
Unequal-arm Michelson X, Y & Z TDIs and its sum $X+Y+Z$ for new LISA

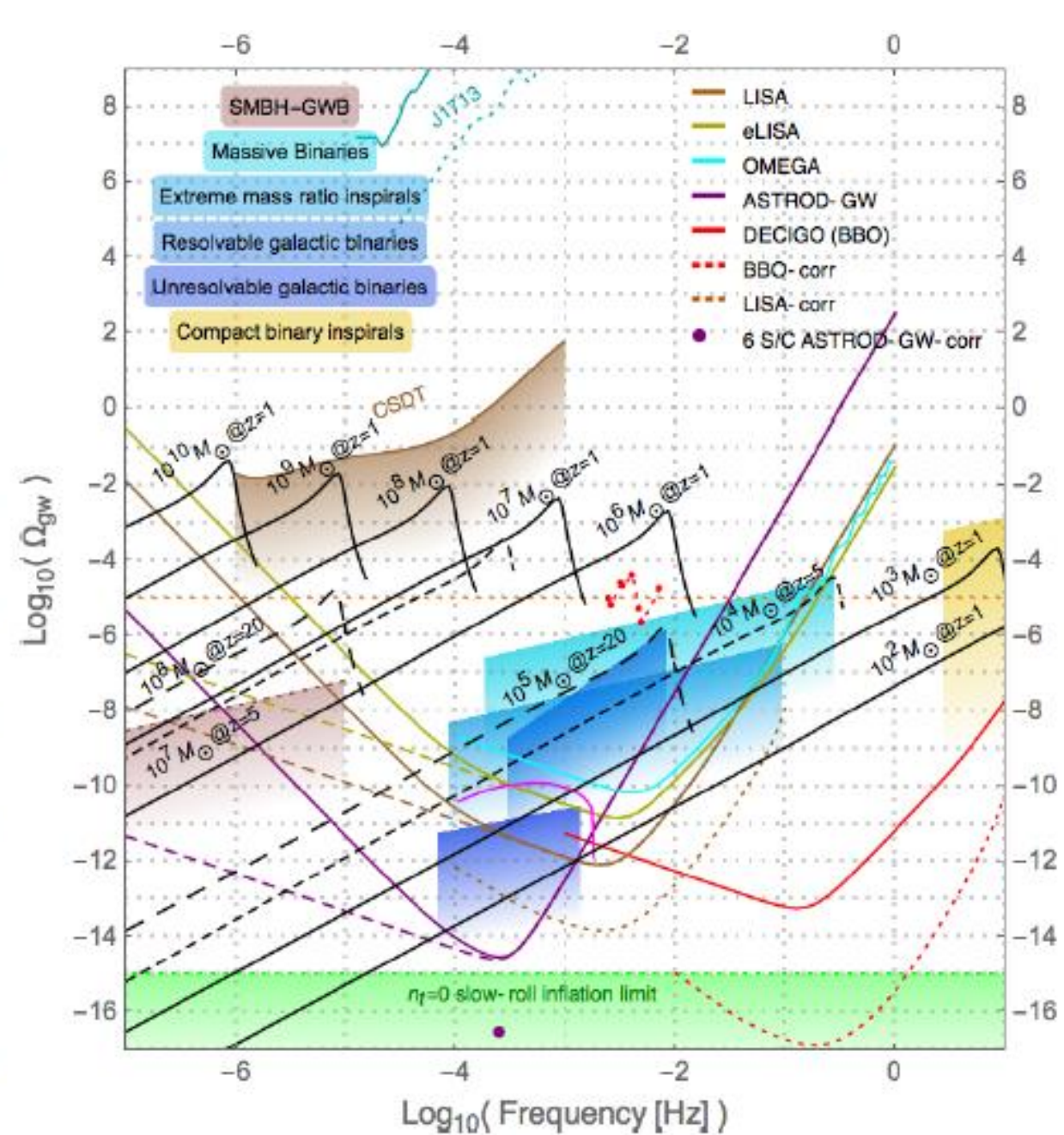
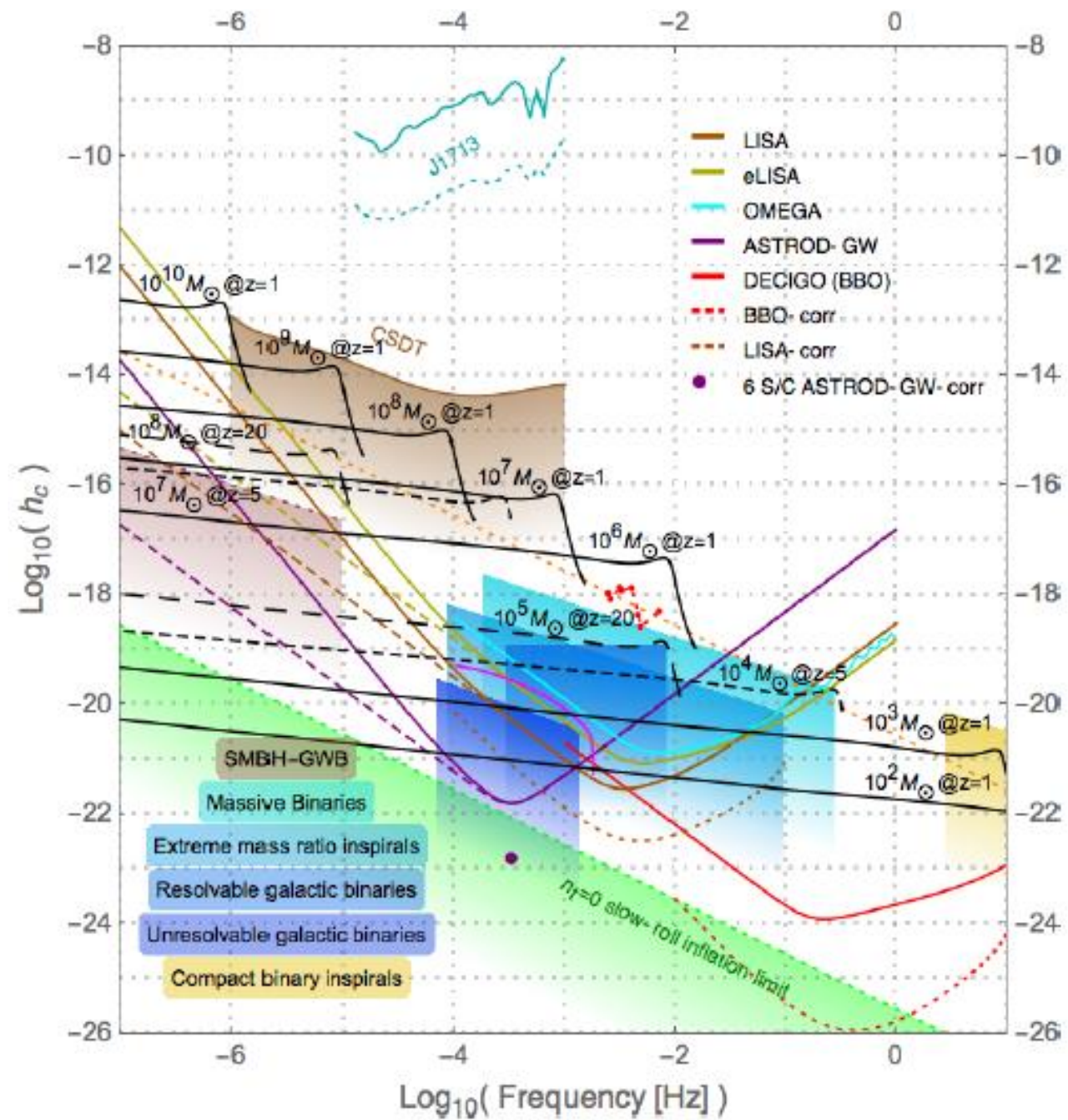
- 1999 Armstrong, Estabrook, Tinto, X, Y & Z TDIs $X+Y+Z$ for LISA
- Vallisneri 2005 (U, P, E)
- Tinto & Dhurandhar review 2014



√ Detection i

Strain power spectral density (psd) amplitude vs. frequency for various GW detectors and GW sources. [CSDT: Cassini Spacecraft Doppler Tracking; SMBH-GWB: Supermassive Black Hole-GW Background.]





Conversion factors among:

the characteristic strain $h_c(f)$,

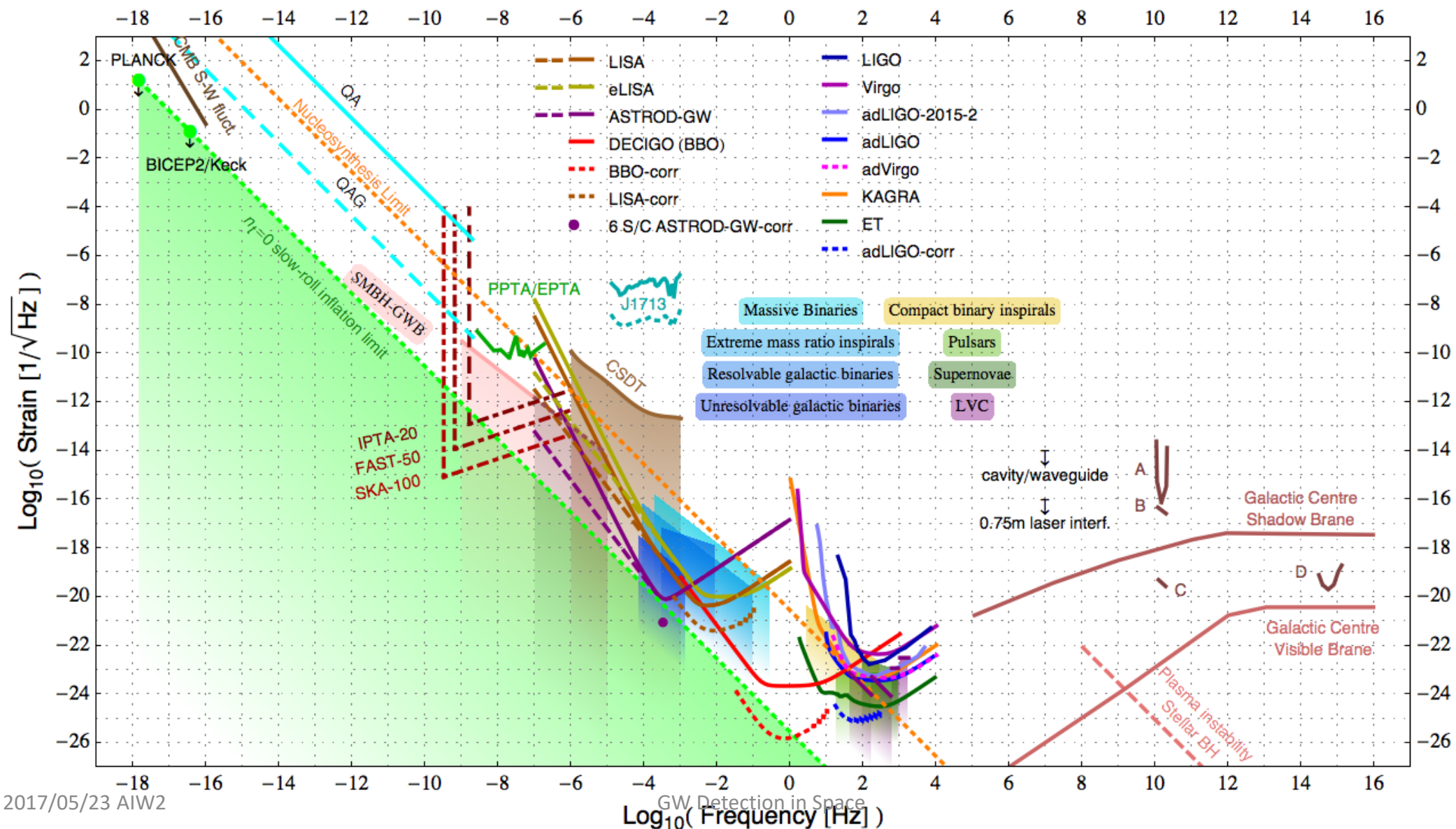
the strain psd (power spectral density) $[S_h(f)]^{1/2}$

the normalized spectral energy density $\Omega_{\text{gw}}(f)$

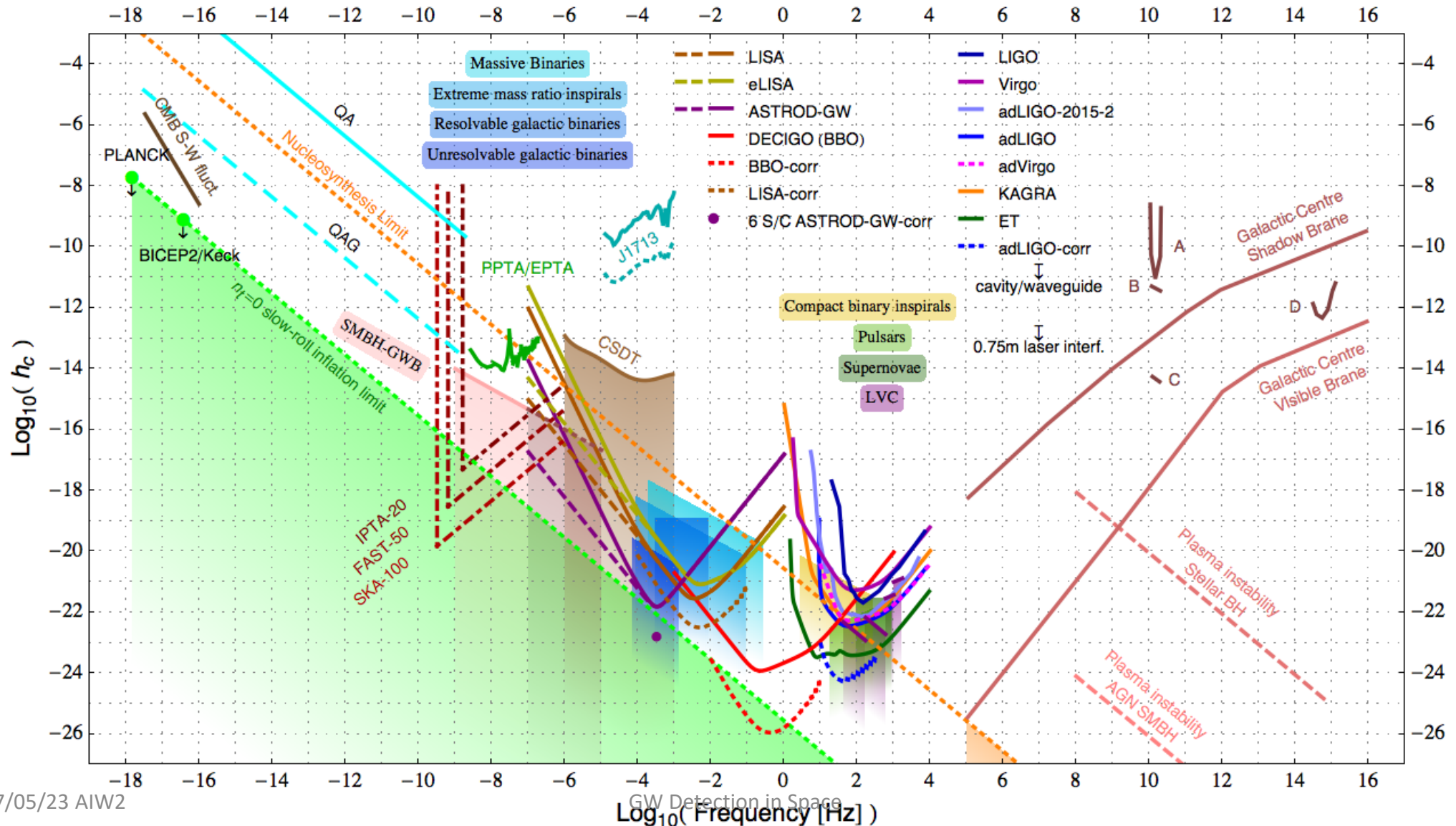
- $h_c(f) = f^{1/2} [S_h(f)]^{1/2}$;
- *normalized GW spectral energy density $\Omega_g(f)$: GW spectral energy density in terms of the energy density per logarithmic frequency interval divided by the cosmic closure density ρ_c for a cosmic GW sources or background, i.e.,*
- $\Omega_{\text{gw}}(f) = (f/\rho_c) d\rho(f)/df$
- $\Omega_{\text{gw}}(f) = (2\pi^2/3H_0^2) f^3 S_h(f) = (2\pi^2/3H_0^2) f^2 h_c^2(f)$.

	Characteristic strain $h_c(f)$	Strain psd $[S_h(f)]^{1/2}$	Normalized spectral energy density $\Omega_{\text{gw}}(f)$
$h_c(f)$	$h_c(f)$	$f^{1/2} [S_h(f)]^{1/2}$	$[(3H_0^2/2\pi^2 f^3)\Omega_{\text{gw}}(f)]^{1/2}$
Strain psd $[S_h(f)]^{1/2}$	$f^{1/2} h_c(f)$	$[S_h(f)]^{1/2}$	$[(3H_0^2/2\pi^2 f^3)\Omega_{\text{gw}}(f)]^{1/2}$
$\Omega_{\text{gw}}(f)$	$(2\pi^2/3H_0^2) f^2 h_c^2(f)$	$(2\pi^2/3H_0^2) f^3 S_h(f)$	$\Omega_{\text{gw}}(f)$

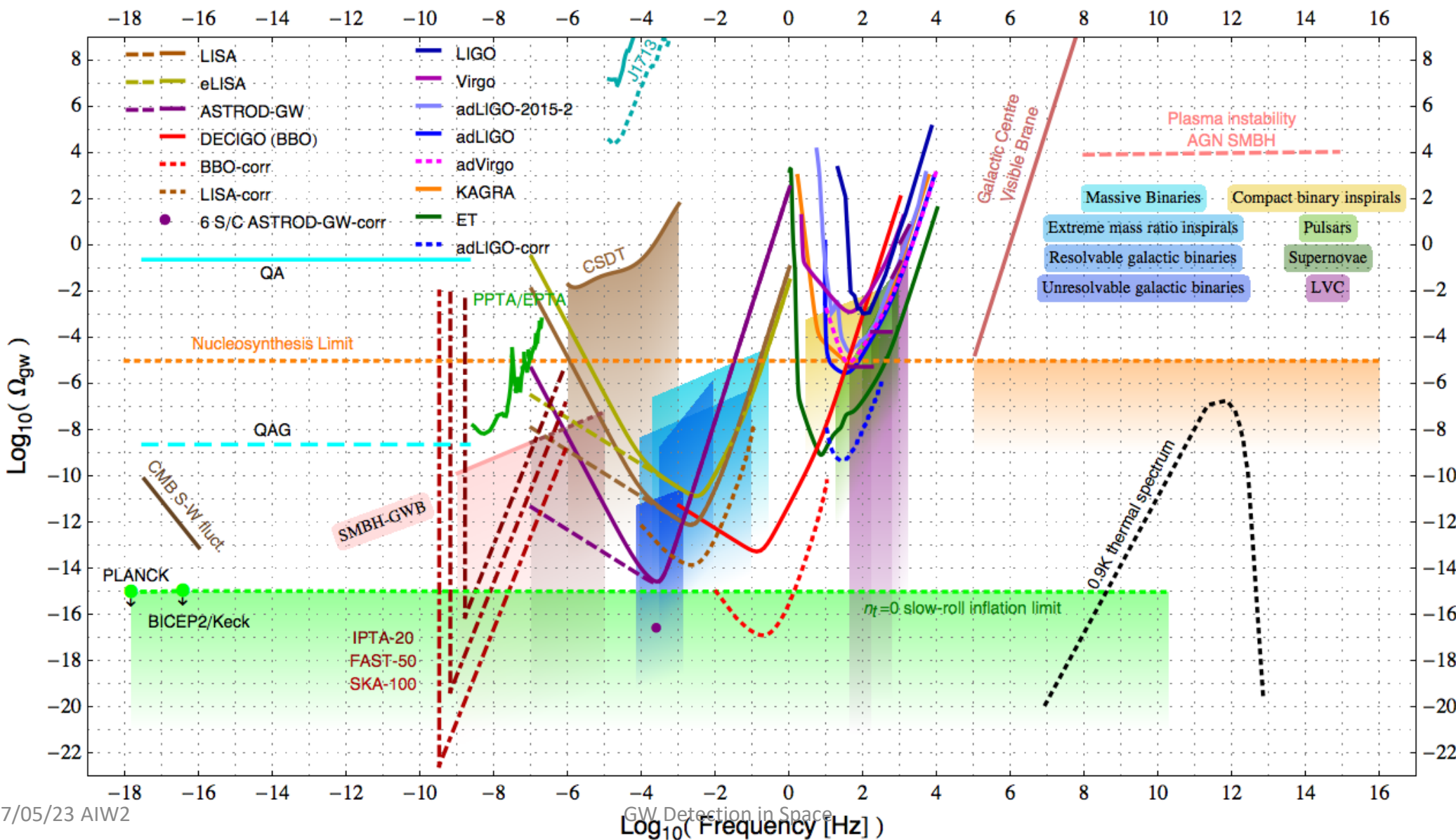
Strain power spectral density (psd) amplitude vs. frequency for various GW detectors and GW sources



Characteristic strain h_c vs. frequency for various GW detectors and sources. [QA: Quasar Astrometry; QAG: Quasar Astrometry Goal; LVC: LIGO-Virgo Constraints; CSDT: Cassini Spacecraft Doppler Tracking; SMBH-GWB: Supermassive Black Hole-GW Background.]



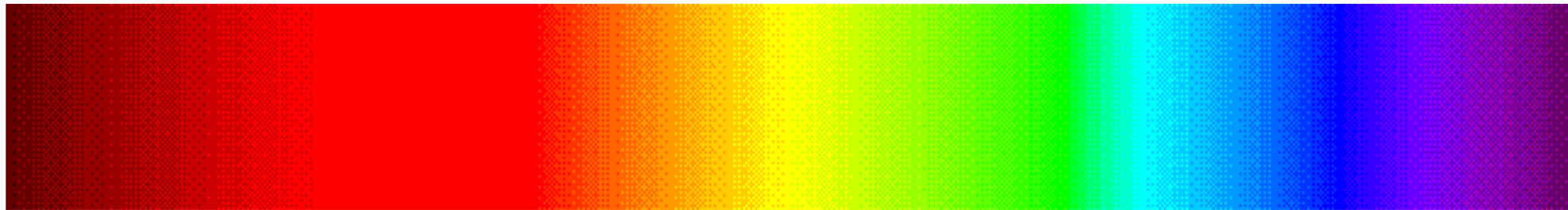
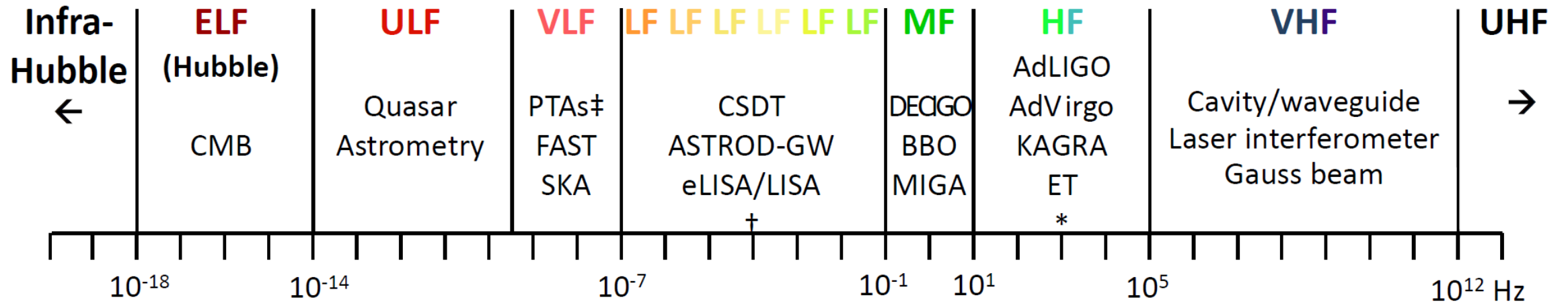
Normalized GW spectral energy density Ω_{gw} vs. frequency for GW detector sensitivities and GW sources



Detection Methods other than Laser Interferometry for Low-frequency and Middle-frequency GWs

- Radio-wave Doppler frequency tracking
- Atom Interferometry involving repeatedly imprinting the phase of optical field onto the motional degrees of freedom of the atoms using light propagating back and forth between the spacecraft.
- Resonant Atom Interferometry detection
- GW detection with optical lattice atomic clocks

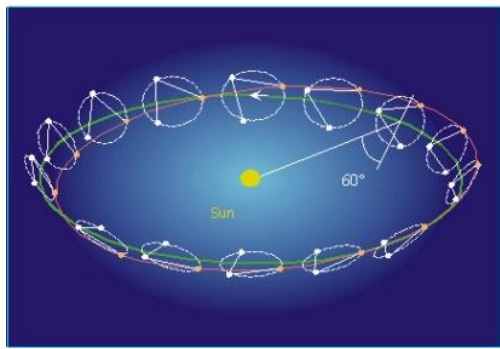
The Gravitation-Wave (GW) Spectrum Classification



* AIGO, AURIGA, EXPLORER, GEO, NAUTILUS, MiniGRAIL, Schenberg.

† OMEGA, gLISA/GEOGRAWI, GADFLI, TIANQIN, ASTROD-EM, LAGRANGE, ALIA, ALIA-descope.

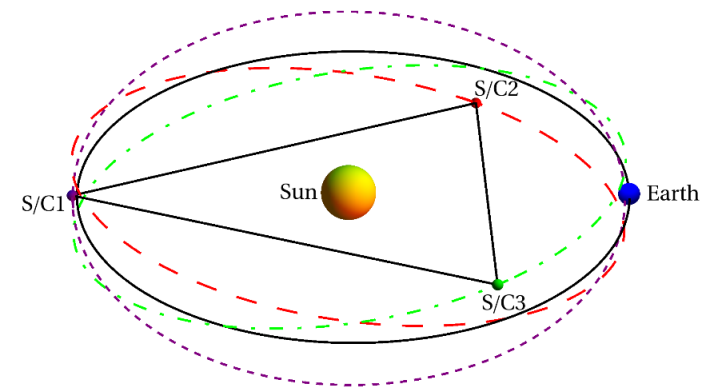
‡ EPTA, NANOGrav, PPTA, IPTA.



A Compilation of GW Mission Proposals

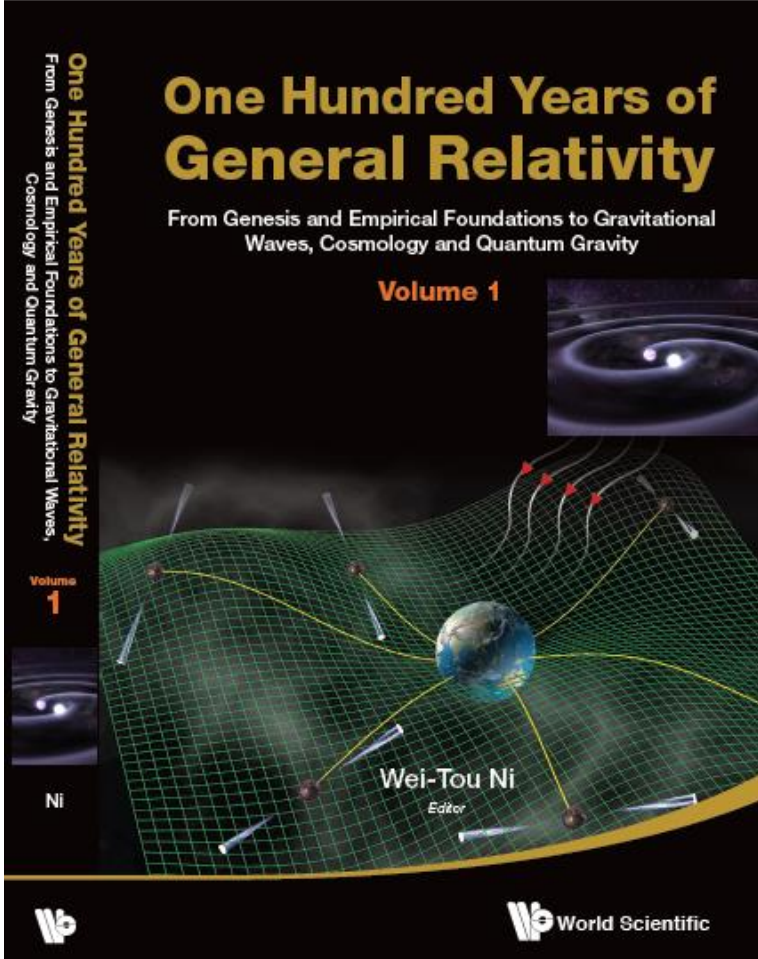
LISA Pathfinder

Launched on December 3, 2015



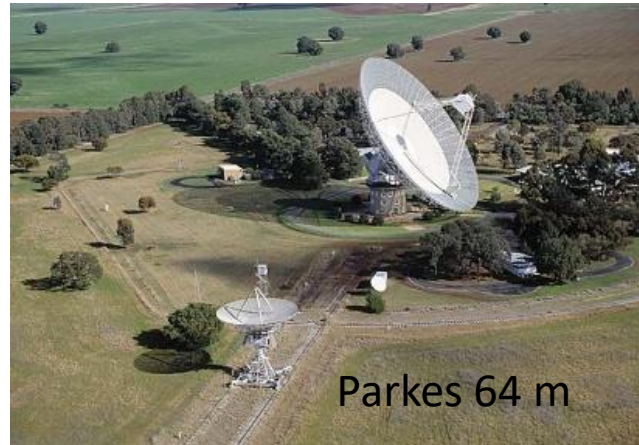
Mission Concept	S/C Configuration	Arm length	Orbit Period	S/C #
<i>Solar-Orbit GW Mission Proposals</i>				
LISA ⁶⁵	Earth-like solar orbits with 20° lag	5 Gm	1 year	3
eLISA ⁶⁴	Earth-like solar orbits with 10° lag	1 Gm	1 year	3
ASTROD-GW ⁶⁸	Near Sun-Earth L3, L4, L5 points	260 Gm	1 year	3
Big Bang Observer ⁷³	Earth-like solar orbits	0.05 Gm	1 year	12
DECIGO ⁷²	Earth-like solar orbits	0.001 Gm	1 year	12
ALIA ⁷⁴	Earth-like solar orbits	0.5 Gm	1 year	3
ALIA-descope ⁷⁵	Earth-like solar orbits	3 Gm	1 year	3
Super-ASTROD ⁷¹	Near Sun-Jupiter L3, L4, L5 points (3 S/C), Jupiter-like solar orbit(s)(1-2 S/C)	1300 Gm	11 year	4 or 5
<i>Earth-Orbit GW Mission Proposals</i>				
OMEGA ⁸¹	0.6 Gm height orbit	1 Gm	53.2 days	6
gLISA/GEOGRAWI ⁷⁶⁻⁷⁸	Geostationary orbit	0.073 Gm	24 hours	3
GADFLI ⁷⁹	Geostationary orbit	0.073 Gm	24 hours	3
TIANQIN ⁸²	0.057 Gm height orbit	0.11 Gm	44 hours	3
ASTROD-EM ^{69,70}	Near Earth-Moon L3, L4, L5 points	0.66 Gm	27.3 days	3
LAGRANGE ⁸⁰	Near Earth-Moon L3, L4, L5 points	0.66 Gm	27.3 days ⁸⁹	3





Pulsar Timing Arrays

PPTA, NANOGrav, EPTA, IPTA
 FAST, SKA



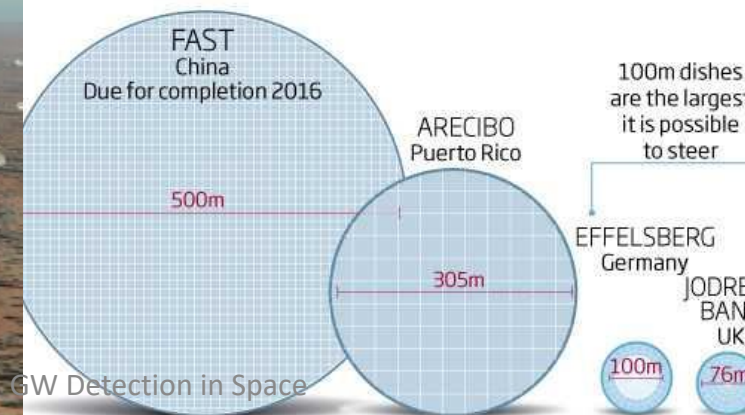
Telescopes go large

©NewScientist

Radio astronomy will get a big boost with FAST, the world's most sensitive radio telescope



SKA Pathfinder



Very low frequency band (300 pHz – 100 nHz)

$$h_c(f) = A_{\text{yr}} [f/(1 \text{ yr}^{-1})]^\alpha$$

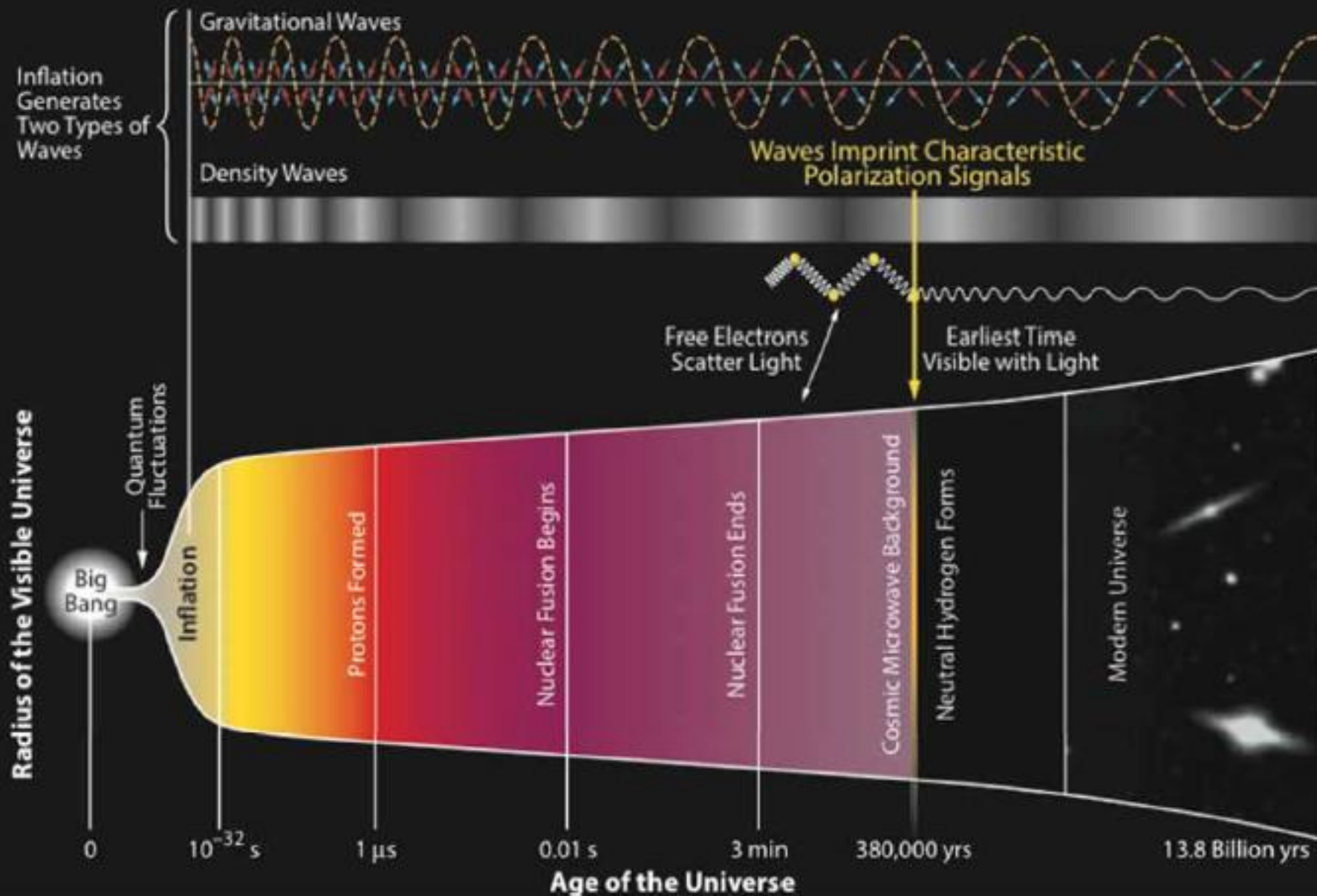
Table 4. Upper limits on the isotropic stochastic background from 3 pulsar timing arrays.

	No. of pulsars included	No. of years observed	Observation radio band [MHz]	Constraint on characteristic strain $h_c(f)$ [= $A_{\text{yr}} [f/(1\text{yr}^{-1})]^{-(2/3)}$, ($f = 10^{-9}$ - 10^{-7} Hz)]
EPTA ¹⁰²	6	18	120-3000	$A_{\text{yr}} < 3 \times 10^{-15}$
PPTA ¹⁰³	4	11	3100	$A_{\text{yr}} < 1 \times 10^{-15}$
NANOGrav ¹⁰⁴	27	9	327-2100	$A_{\text{yr}} < 1.5 \times 10^{-15}$

Table 5. Sensitivities of IPTA, FAST and SKA to monochromatic GWs.

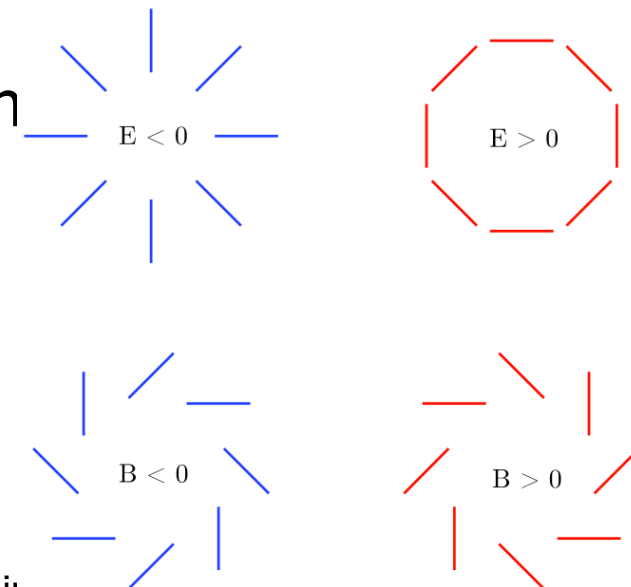
	No. of pulsars	No. of years of observation	Timing accuracy (ns)	Sensitivity in characteristic strain $h_c(f)$ [= $B_{\text{yr}} (f/\text{yr}^{-1})$] for monochromatic GWs
IPTA ¹⁰⁶	36	20	100	$B_{\text{yr}} = 1 \times 10^{-16}$
FAST ¹⁰⁷	50	50	50	$B_{\text{yr}} = 1.5 \times 10^{-17}$
SKA ¹⁰⁸	100	100	20	$B_{\text{yr}} = 1.5 \times 10^{-18}$

History of the Universe



Four processes could produce CMB B-mode polarization observed

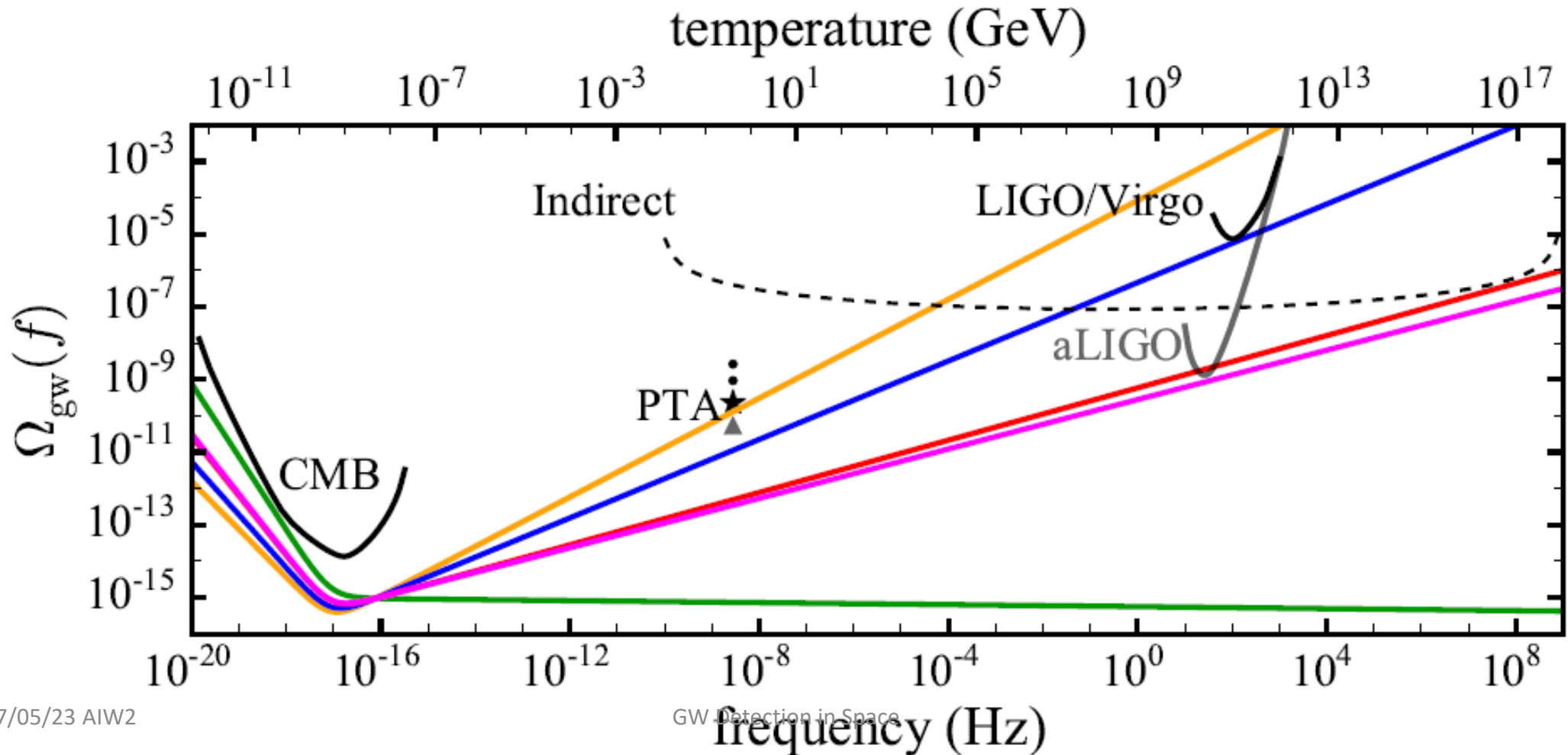
- (i) gravitational lensing from E-mode polarization (Zaldarriaga & Seljak 1997),
- (ii) **local quadrupole anisotropies in the CMB** within the last scattering region by large scale GWs (Polnarev 1985)
- (iii) **cosmic polarization rotation (CPR)** due to pseudoscalar-photon interaction (Ni 1973; for a review, see Ni 2010).
(The CPR has also been called **Cosmological Birefringence**)
- (iv) **Dust alignment**



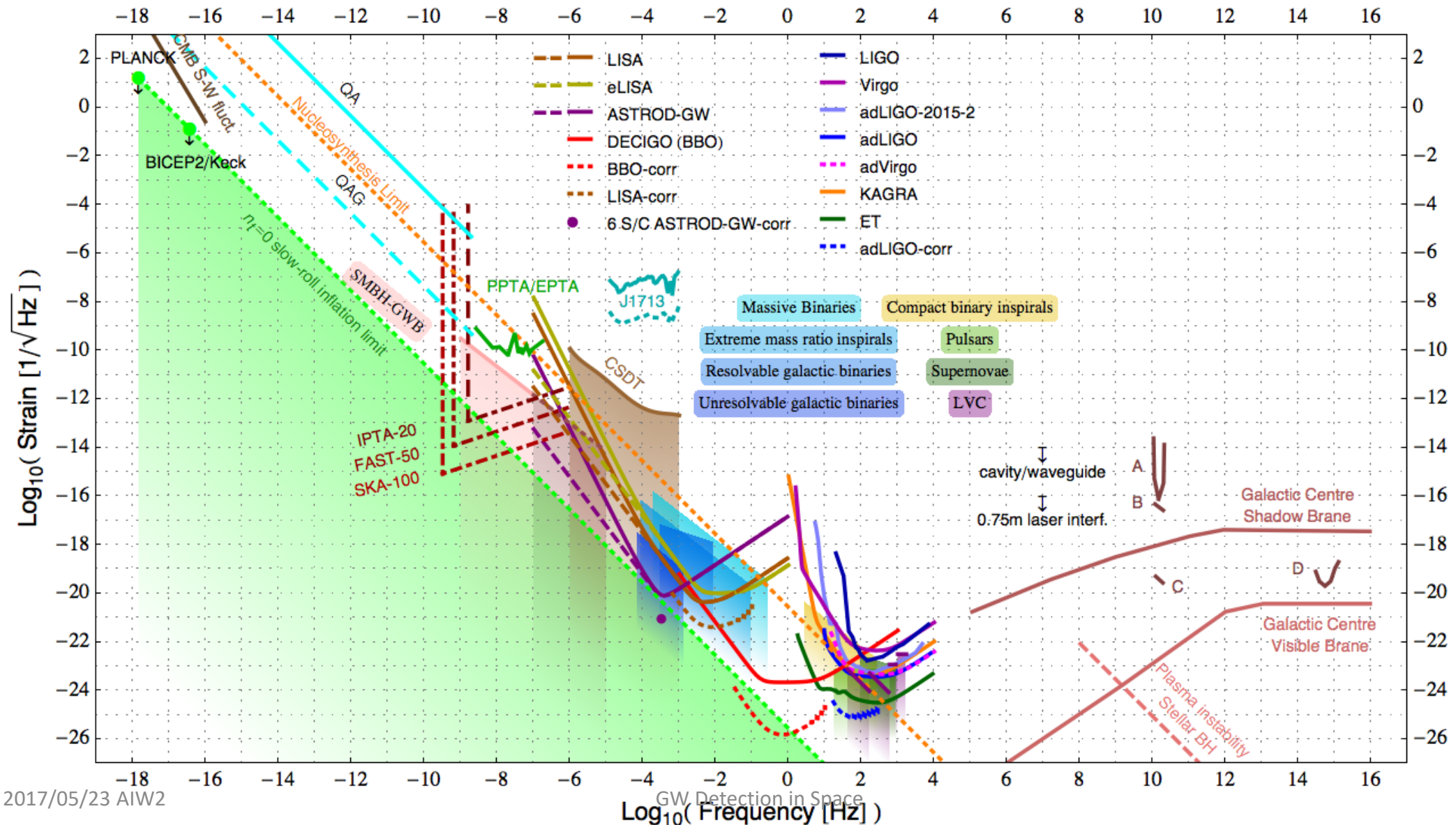
The constraints for Hubble frequency band

- CMB S-W fluct.: The COBE microwave-background quadrupole anisotropy measurement gives a limit $\Omega_{\text{gw}} (1 \text{ aHz}) \sim 10^{-9}$ on the extremely-low-frequency GW background.
- WMAP improves on the COBE constraints; the constraint on Ω_{gw} for the higher frequency end of this band is better than 10^{-14} .
- The analysis of *Planck*, SPT, and ACT temperature data together with WMAP polarization; the scalar index is $n_s = 0.959 \pm 0.007$, the tensor-to-scalar perturbation ratio r is less than 0.11
- The combined analysis of BICEP2/Keck Array and Planck Collaboration: the tensor-to-scalar perturbation ratio r is constrained to less than 0.12 (95% CL; no running). The pivot scale of this constraint is 0.05 Mpc^{-1} , corresponding to GW frequency f at 3.8×10^{-17} Hz at present.
- Most recent: $r < 0.07$ (2σ) (Chao-Lin Kuo, Dec. 9 talk at NCTS; his talk in LeCosPA Symposium 12/17/15)

The indirect GW limits are from CMB temperature and polarization power spectra, lensing, BAOs, and BBN. Models predicting a power-law spectrum that intersect with an observational constraint are ruled out at $> 95\%$ confidence. We show five predictions for the GW background, each with $r = 0:11$, and with $nt = 0:68$ (orange curve), $nt = 0:54$ (blue), $nt = 0:36$ (red), $nt = 0:34$ (magenta), and the consistency relation, $nt = r/8$ (green), corresponding to minimal inflation. Paul D. Lasky et al.1511.05994



Strain power spectral density (psd) amplitude vs. frequency for various GW detectors and GW sources



Outlook

First generation

- LISA Pathfinder, LISA
- TAIJI, TIANQIN
- B-DECIGO
- ASTROD-GW

Second generation

- BBO, DECIGO
- Super-ASTROD

Outlook

- Advanced LIGO has detected GWs from stellar-mass binary black hole mergers. We will see a global network of second generation km-size interferometers for GW detection soon. Scaling with the achieved detection, third generation detectors would be to detect more than 100,000 5- σ GW events per year.
- Advanced LIGO has achieved 3.5 times better sensitivities with a reach to neutron star binary merging event at 70 Mpc and began its first observing run (O1) on September 18, 2015 searching for GWs.
- Another avenue for real-time direct detection is from the PTAs. The PTA bound on stochastic GW background already excludes most theoretical models; this may mean we could detect very low frequency GWs anytime too with a longer time scale.
- Although the prospect of a launch of space GW is only expected in about 20 years, the detection in the low frequency band may have the largest signal to noise ratios. This will enable the detailed study of black hole co-evolution with galaxies and with the dark energy issue. **LISA Pathfinder has been launched on December 3, 2015.** This will **pave the technology road for GW space missions.**
- **Foreground separation and correlation detection method** need to be investigated to achieve the sensitivities 10^{-16} - 10^{-17} or beyond in Ω_{gw} to study the primordial GW background for **exploring very early universe and possibly quantum gravity regimes.**

Thank
You